epartment
nsportation
ral Railroad
inistration

Growth Life of Surface Cracks in the Rail Web

e of Research and
elopment
nington, DC 20590

D. Y. Jeong

Institute of Fracture and Solid Mechanics
Lehigh University
Bethlehem, Pennsylvania 18015

FRA/ORD-89/
TSC-FRA-89-1

January 1989
Final Report

Technical Report Documentation Page

1. Report No.	2. Government Accession No.	3. Recipient's Catalog No.
DOT/FRA/ORD-89/		

4. Title and Subtitle
GROWTH LIFE OF SURFACE CRACKS IN THE RAIL WEB

5. Report Date: January 1989
6. Performing Organization Code: DTS-76

7. Author(s)
D. Y. Jeong

8. Performing Organization Report No.: DOT-TSC-FRA-89-1

9. Performing Organization Name and Address
Institute of Fracture and Solid Mechanics**
Lehigh University
Bethlehem, PA 18015

10. Work Unit No. (TRAIS): RR919/R9003
11. Contract or Grant No.: DTRS-57-85-C-00093

12. Sponsoring Agency Name and Address
U.S. Department of Transportation
Federal Railroad Administration
Office of Research and Development
Washington, DC 20590

13. Type of Report and Period Covered: Final Report
November 1987 - November 1988

14. Sponsoring Agency Code: RRS-30

15. Supplementary Notes
*Under contract to: U.S. Department of Transportation
Research and Special Programs Administration
Transportation Systems Center
Cambridge, MA 02142

16. Abstract

The results of a theoritical study of the propagation behavior of surface cracks in the web of railroad rails are presented. Two fracture mechanics models are presented: 1) a conventional LEFM model of an elliptical surface crack of constant aspect ratio growing through the web thickness; and (2) a generalized surface crack model based on Sih's strain energy diversity approach. The conventional model predicts that the crack will propogate only at extremely slow rates, even under conditions of tensile vertical residual stress created by roller straightening. The strain energy diversity model predicts a slow propogation principally along the web (i.e., the crack aspect ratio increases) without residual stress.

17. Key Words	18. Distribution Statement
Crack Growth, Fracture Mechanics, Rail Integrity, Safe Crack Growth Life, Split Web, Surface Crack	DOCUMENT IS AVAILABLE TO THE PUBLIC THROUGH THE NATIONAL TECHNICAL INFORMATION SERVICE, SPRINGFIELD, VIRGINIA 22161

19. Security Classif. (of this report)	20. Security Classif. (of this page)	21. No. of Pages	22. Price
UNCLASSIFIED	UNCLASSIFIED	54	

Form DOT F 1700.7 (8-72)

PREFACE

This report summarizes analytical research on the propagation behavior of surface cracks in the webs of railroad rails. The work was sponsored by the Office of Research and Development of the Federal Railroad Administration (FRA) as a part of the FRA Track Safety Research Program. The work was monitored by the Structures and Dynamics Division, U.S. DOT Transportation Systems Center.

Approximate Conversions to Metric Measures

Symbol	When You Know	Multiply by	To Find	Symbol
		LENGTH		
in	inches	*2.5	centimeters	cm
ft	feet	30	centimeters	cm
yd	yards	0.9	meters	m
mi	miles	1.6	kilometers	km
		AREA		
in^2	square inches	6.5	square centimeters	cm^2
ft^2	square feet	0.09	square meters	m^2
yd^2	square yards	0.8	square meters	m^2
mi^2	square miles	2.6	square kilometers	km^2
	acres	0.4	hectares	ha
		MASS (weight)		
oz	ounces	28	grams	g
lb	pounds	0.45	kilograms	kg
	short tons (2000 lb)	0.9	tonnes	t
		VOLUME		
tsp	teaspoons	5	milliliters	ml
Tbsp	tablespoons	15	milliliters	ml
fl oz	fluid ounces	30	milliliters	ml
c	cups	0.24	liters	l
pt	pints	0.47	liters	l
qt	quarts	0.95	liters	l
gal	gallons	3.8	liters	l
ft^3	cubic feet	0.03	cubic meters	m^3
yd^3	cubic yards	0.76	cubic meters	m^3
		TEMPERATURE (exact)		
°F	Fahrenheit temperature	5/9 (after subtracting 32)	Celsius temperature	°C

*1 in. = 2.54 cm (exactly). For other exact conversions and more detail tables see NBS Misc. Publ. 286, Units of Weight and Measures. Price $2.25 SD Catalog No. C13 10 286.

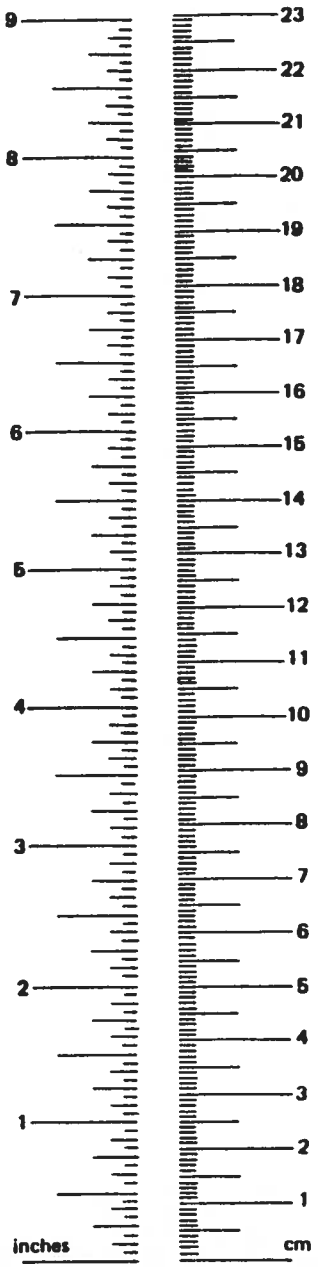

Approximate Conversions from Metric Measures

Symbol	When You Know	Multiply by	To Find	Symbol
		LENGTH		
mm	millimeters	0.04	inches	in
cm	centimeters	0.4	inches	in
m	meters	3.3	feet	ft
m	meters	1.1	yards	yd
km	kilometers	0.6	miles	mi
		AREA		
cm^2	square centimeters	0.16	square inches	in^2
m^2	square meters	1.2	square yards	yd^2
km^2	square kilometers	0.4	square miles	mi^2
ha	hectares (10,000 m^2)	2.5	acres	
		MASS (weight)		
g	grams	0.035	ounces	oz
kg	kilograms	2.2	pounds	lb
t	tonnes (1000 kg)	1.1	short tons	
		VOLUME		
ml	milliliters	0.03	fluid ounces	fl oz
l	liters	2.1	pints	pt
l	liters	1.06	quarts	qt
l	liters	0.26	gallons	gal
m^3	cubic meters	36	cubic feet	ft^3
m^3	cubic meters	1.3	cubic yards	yd^3
		TEMPERATURE (exact)		
°C	Celsius temperature	9/5 (then add 32)	Fahrenheit temperature	°F

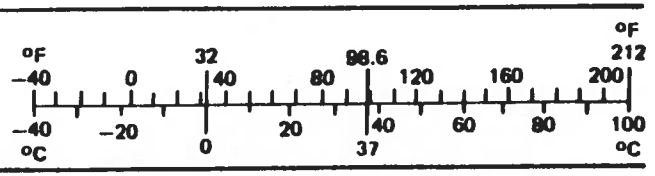

TABLE OF CONTENTS

LIST OF ILLUSTRATIONS

LIST OF TABLES

EXECUTIVE SUMMARY

This report summarizes a theoretical study of the behavior of surface cracks in the webs of railroad rails. The study was motivated by recent reports of rail failures caused by web cracks which had apparently grown at unusually rapid rates. The rapid growth had possibly been caused by the presence in the rail of residual stress from a roller-straightening process. (Rails were generally not roller straightened in older U.S. production, which was in service when the present rail inspection intervals were established.)

The objective of the present study was to make comparative estimates of web surface crack growth rates with and without residual stress present. A linear elastic fracture mechanics (LEFM) model of a semi-elliptical surface crack was used to make the comparison. The semi-elliptical surface crack represents typical characteristics of initial damage which might be caused on rail webs by excessively severe brand stamping at the mill or by accidental blows from a rail spike maul during installation. The LEFM type of model has been successfully applied to other kinds of rail defects, such as transverse cracks in the head.

In the present case, the LEFM model was used to estimate the life for an initial surface crack to enlarge until its deepest point would penetrate through the web thickness. The LEFM model estimates were found to exceed the rail service life by a factor of at least 10 to 20, even when a large value was assumed for roller-straightening residual stress. Accordingly, the LEFM model for this type of rail defect was judged to be invalid.

An alternative model based on three-dimensional finite element analysis and the strain energy density formulation of fracture mechanics was also applied to the problem. This model also starts with a semi-elliptical surface crack, but the strain energy density formulation allows crack-shape changes to be computed during the growth calculation. Only the case of rail with no residual stress could be analyzed within the funds available for the study. The results of these calculations showed that the most rapid growth would be expected to occur along the rail web surface (rather than through the thickness as assumed for the LEFM model), and the estimated lifetimes were of the order of one half a typical rail service life or less.

1. INTRODUCTION

The Transportation Systems Center has supported the Federal Railroad Administration in its track safety research program for the past several years. Among the projects in the track safety program is one concerning rail integrity. The objective of the rail integrity project is to identify practical approaches to the reduction of derailments caused by rail failures. Various types of defects, if not detected by inspection, can cause rail failures. A review on the objectives and investigations of the rail integrity project can be found in Reference 1.

Within the past two years, some unexplained incidents of split web failures have occurred in the Northeast Corridor track. These failures pose safety risks due to the high speed of train operations in the corridor and due to the high volume of passenger traffic on this line.

The rail failures originate as semi-elliptical surface fatigue cracks on either the field side or gage side of the rail. Figure 1 illustrates the typical crack location and orientation. Two possible sources of cracking have been identified: (1) production stamp markings (where such markings are made more severely than normal); and (2) damage induced when a rail web is accidentally struck by a spike maul. The initial crack appears to propagate through the web thickness (i.e., field to gage side or vice versa) before transition to a split web through crack. Under normal circumstances, a flaw of this type grows slowly enough so that it can be detected while still a surface crack by ultrasonic rail testing performed in accordance with existing inspection schedules. Detection in the surface crack regime is essential because propagation to failure can be extremely rapid once the through crack regime is entered.

In the present case, however, it appears that the surface crack regime is also subject to accelerated propagation, and the flaws are thus able to reach the through crack stage ahead of the rail test. A possible reason for the anomalous behavior is that the rails in the present case are roller-straightened, whereas previous experience of successful web surface crack detection has been based on nonroller-straightened rails. The roller-straightening process is known to create residual stresses in rails.

In this study, the sensitivity of surface crack growth life to the combination of web residual stress and live load stresses is investigated. The purpose of this report is to present some results on this sensitivity study. Two approaches are undertaken in this investigation. The first approach uses an engineering

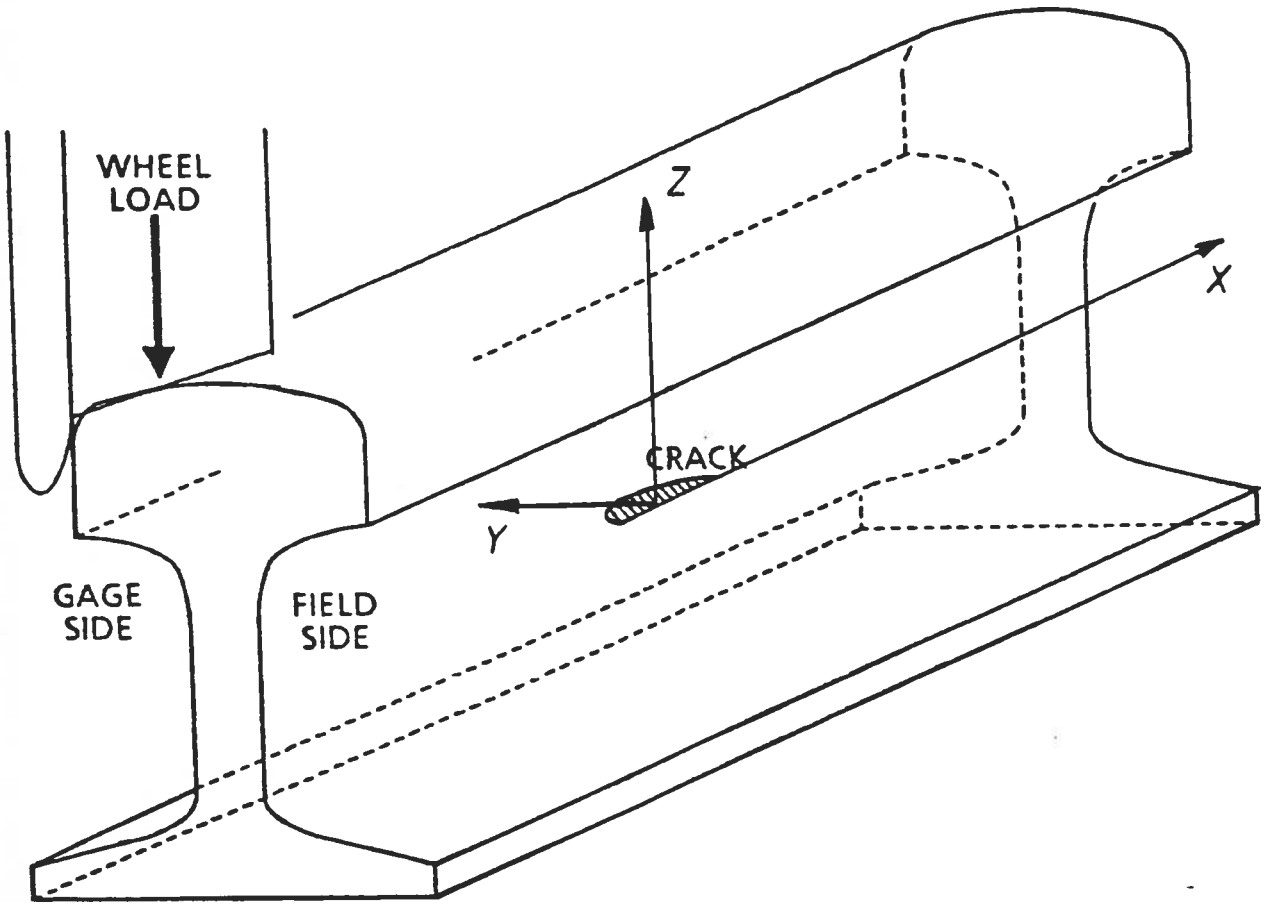

FIGURE 1. CRACK LOCATION AND ORIENTATION

fracture mechanics model. The web crack is modeled as a semi-elliptical crack in a semi-infinite medium. The stress intensity factor for this type of crack can be found in handbook (for example, Reference 2). With the aid of an appropriate choice of a crack growth relation, the crack size in terms of the ratio of the length of the semi-minor axis of the semi-elliptical crack to rail web thickness versus life in terms of million gross tons can be calculated. This approach has also been used in modeling the growth of detail fractures in the head of rail [3]. The second approach uses the strain energy density criterion to model the surface crack as a crack which can grow in a non-self-similar manner. Initially, the crack is assumed as a semi-elliptical surface crack. As the crack grows, the amount of extension is determined by the energy density criterion. This approach has also been used in previous studies of other rail defects such as the detail fracture and the bolt hole crack [4,5].

2. ENGINEERING FRACTURE MECHANICS MODEL

An engineering fracture mechanics model is presented in this section. The model is comprised of two major parts: (1) one-dimensional stress analysis and (2) crack growth analysis based on conventional linear elastic fracture mechanics. In particular, the concept of stress intensity factor is used for subcritical fatigue crack growth. The model considers only Mode I crack growth. Loading is characterized by a load spectrum which is translated into stress data. The material of the rail is characterized by crack growth rate constants.

A simplified load spectrum based on an isolated 33-kip wheel load is used for the present study. Dynamic effects are considered by multiplying the static wheel load by factors. A load schedule for one train is given in Table 1. It can be seen that the loads given in the table correspond to 13,392 gross tons for one train.* (It should be noted that 416 static wheel loads with an average value of 33 kips actually correspond to 13,728 gross tons. In the subsequent calculations, the value of 13,392 gross tons was used. Therefore, the predicted lives will be 3 percent higher than if the static gross tonnage had been used.) The resulting dynamic histogram accounts only for vertical wheel loads, however. Lateral loading is assumed to be a function of the track curvature. That is, wheel loads on tangent tracks are subjected to relatively low lateral loads compared to curved tracks. Also, lateral wheel loads are assumed to be a fraction of the applied vertical wheel load. The ratio of lateral-to-vertical wheel load or L/V is assumed to be 0.05 for tangent track and to vary between 0.15 and 0.30 for curved tracks.

From the simplified load spectrum, the vertical stress component associated with each wheel load is calculated as a function of the longitudinal distance along the track. The minimum and maximum stresses can then be determined from the stress distribution. These min/max pairs are then used to define mean and alternating stress components which are required for the calculation of crack growth life. It is assumed that each wheel load creates one pair of minimum and maximum stresses. In other words, each wheel load is assumed to create one stress cycle.

*The figure given is actually a summation of the assumed dynamic loads. For practical purposes, the gross tonnage would normally be based on static load (i.e., 13,728 tons in the present case, based on 33 tons per axle). However, the difference in the present case is only 3 percent, and the calculated results have not been adjusted.

TABLE 1. LOAD SCHEDULE FOR ONE TRAIN

Group	Number of loads	Dynamic Value of Wheel Load (kips)
1	96	26
2	208	33
3	112	36
Total	416	--

2.1 STRESS ANALYSIS

The stresses in rails have been determined in previous studies of rail defects (References 3 and 8, for example) by using analyses developed by Timoshenko and Langer [6]. However, these analyses consider only the longitudinal component of stress. In the present model, the relevant component of stress which must be calculated is the vertical stress since only the opening mode of crack propagation is assumed. Therefore, other analyses must be developed in order to determine the vertical stress in the rail web.

There are three sources from which the vertical stress component is comprised: (1) due to vertical load, (2) due to bending of the web by a moment resulting from eccentric vertical load and/or lateral load, and (3) residual stress. The total vertical stress at a given point in the web cross section is assumed to be the superposition of these three different effects.

The component due to vertical load is calculated using the beam on elastic foundation theory [7]. This component has a uniform distribution across the web thickness and is roughly estimated as the product of rail deflection and foundation modulus divided by the web thickness. A more accurate determination of this stress component can be made by modeling the rail web as a long plate with finite thickness and height, (see Figure 2). The plate is loaded on the bottom by a vertical stress distribution due to the rail foundation modulus. This stress distribution can be calculated for a single concentrated vertical load, P, applied at the origin by the following:

$$\sigma_{zz}(x,-c) = \frac{P\lambda_1}{2t_w} e^{-\lambda_1 x}(\cos\lambda_1 x + \sin\lambda_1 x) \qquad (1)$$

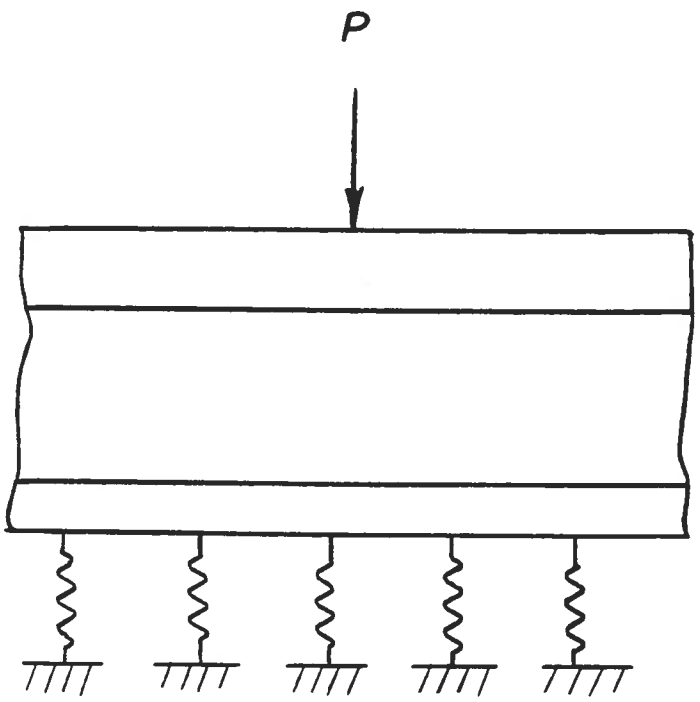

(a) RAIL AS A BEAM ON ELASTIC FOUNDATION

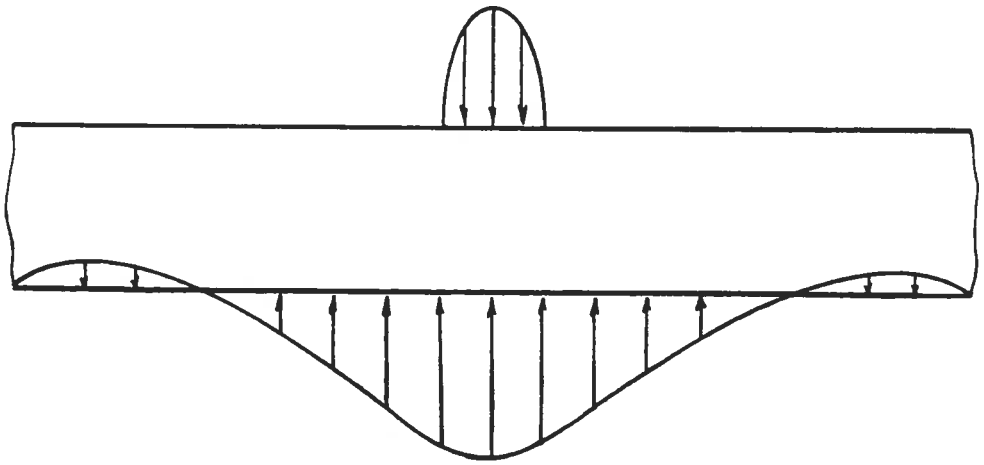

(b) RAIL WEB LOADED BY STRESS DISTRIBUTION

FIGURE 2. RAIL WEB VERTICAL STRESS MODEL

$$\lambda_1^4 = \frac{k}{4EI_{yy}}$$

In this equation, E is Young's modulus, I_{yy} is the area moment of inertia for vertical bending, k is the rail vertical foundation modulus, t_w is the thickness of the web, and c is half the height of the rail web or $h_{w/2}$. Similarly, the top of the plate is loaded by a vertical stress distribution created by the so-called head on web effect:

$$\sigma_{zz}(x, +c) = \frac{P\lambda_2}{2t_w} e^{-\lambda_2 x} (\cos \lambda_2 x + \sin \lambda_2 x) \qquad (2a)$$

$$\lambda_2^4 = \frac{k_{wv}}{4EI_{yyh}} \text{ and } k_{wv} = \frac{Et_w}{h_w} \qquad (2b)$$

In this case, k_{wv} is the effective vertical web modulus defined by Timoshenko and Langer [6] and I_{yyh} is the area moment of inertia for vertical bending of the rail head only. Thus, the problem is reduced to one that can be easily solved by applying elasticity methods [8]. A closed form solution for a plate of length L is obtained by using Fourier series and is given by:

$$\sigma_{zz(1)}(x,z) = \sum_{m=0}^{\infty} -(A_m+B_m)\left(\frac{[\alpha c \cosh \alpha c + \sinh \alpha c]\cosh \alpha z}{\Delta_1} - \frac{\alpha y \sinh \alpha c \sinh \alpha z}{\Delta_1}\right)\cos \alpha x$$

$$+ \sum_{m=0}^{\infty} (A_m - B_m)\left(\frac{[\alpha c \sinh \alpha c + \cosh \alpha c]\sinh \alpha z}{\Delta_2} - \frac{\alpha z \cosh \alpha c \cosh \alpha z}{\Delta_2}\right)\cos \alpha x$$

$$\Delta_1 = \sinh 2\alpha c + 2\alpha c\,,\ \Delta_2 = \sinh 2\alpha c - 2\alpha c\,, \text{ and } \alpha = m\pi/L. \qquad (3)$$

The Fourier coefficients, A_m and B_m are determined from the applied vertical stress distributions on the lower and upper edges of the plate given in equations (1) and (2), respectively. However, these stress distributions must be expressed in terms of an infinite Fourier series. The derivation of the Fourier coefficients required for the calculation of this component of vertical stress is presented in Appendix A. For computational purposes, the series was truncated at 250 terms. The variation of this component of the vertical stress as given in equation (3) is shown in Figure 3 for a single concentrated load. It can be seen from this figure that at the center of the plate the stress distribution varies such that the sign of the stress changes at some distance from the applied load. This is called the reversed bending phenomenon. The ratio of the maximum tensile stress to the maximum compressive stress at the center of the plate is 0.043. Note that this value, however, depends on the location of z (see Figure 3). For the web crack problem, the location of interest is at the center of the web.

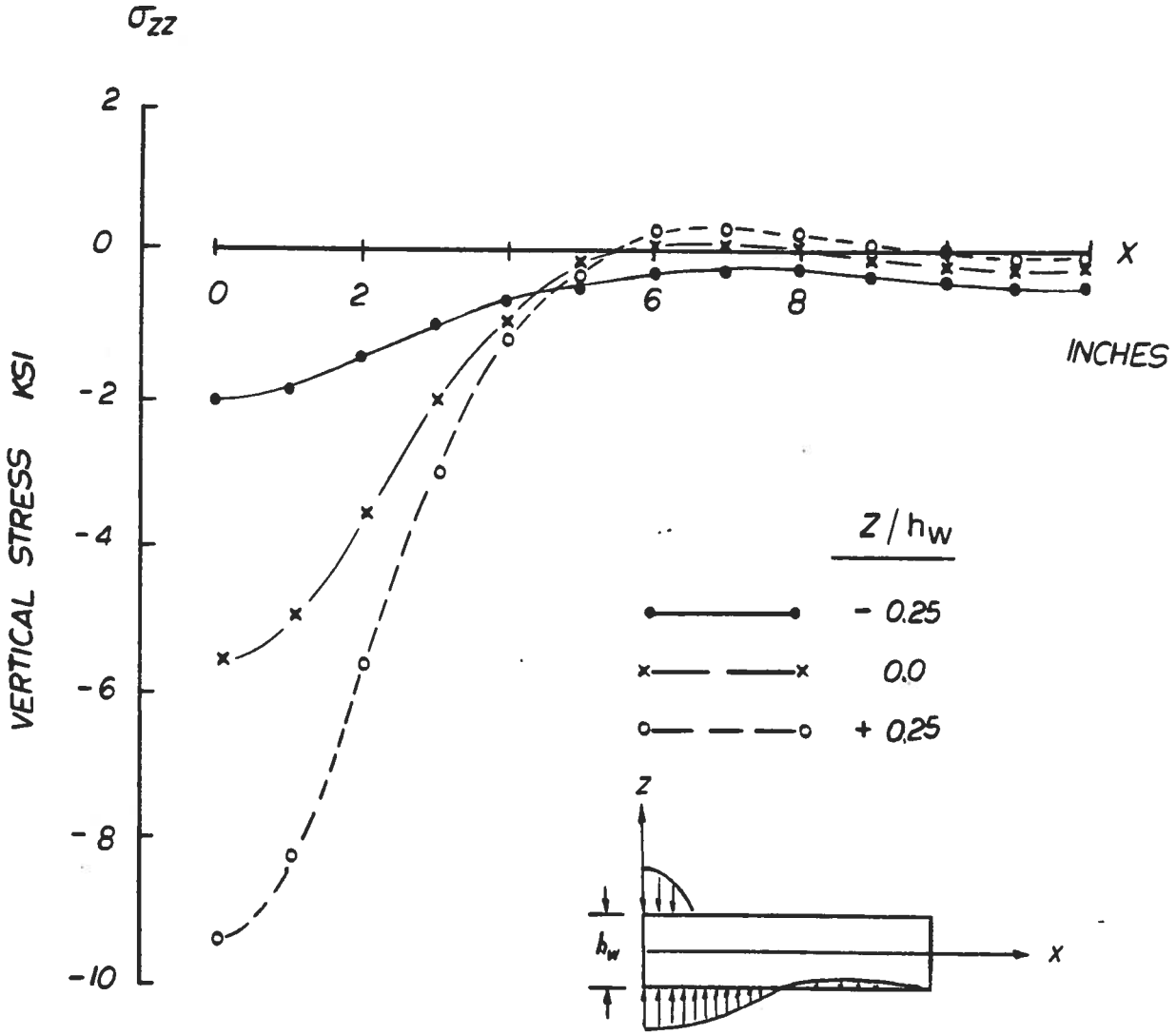

FIGURE 3. VARIATION OF VERTICAL STRESS DUE TO VERTICAL WHEEL LOAD

The effect of eccentric vertical wheel load and/or lateral load is also handled through elasticity methods. The offset vertical load and lateral load combination is resolved into a statically equivalent moment applied at the bottom of the rail head or the top of the web of the rail. Referring to Figure 4, this moment is calculated as:

$$M = V\left(e - \frac{L}{V} f^*\right) \tag{4}$$

where V is the applied vertical load, L is the applied lateral load, e is the vertical eccentricity and f* is the distance between the load application point and the top of the rail web. The rail web is then modeled as an infinitely long cantilever plate subjected to a concentrated moment at the origin. Jaramillo presented a closed form solution to the problem of an infinite cantilever plate subjected to a transverse concentrated load [9]. The solution was given in terms of improper integrals for deflections and moments which were then transformed into series form by the use of contour integration and residue calculus. A solution to the problem of an infinite plate loaded by a concentrated moment can be obtained in a similar manner by merely altering the relevant boundary conditions. Figure 5 shows some results of such an analysis. In this figure, the variation of moment along the longitudinal length of the plate is shown at different depths of the plate. It is interesting to see that the moment does not reverse in sign at any distance from the point of application. The derivation of the expressions which have been altered from Reference 9 is given in Appendix B. Once the moment M_z at a particular location is known, the vertical stress component due to offset vertical load and lateral load is calculated from small deflection plate theory. Thus, this component of the vertical stress varies linearly across the web thickness:

$$\sigma_{zz\,(2)} = \frac{12\, M_z\, y}{t^3} \tag{5}$$

The third source of vertical stress is the residual stress. As mentioned previously, residual stresses can develop in roller-straightened rails during the manufacturing process. Experimental measurements have shown that there exists a compressive vertical stress on the web surface. Equilibrium considerations imply that a distribution of vertical residual stress must exist through the web thickness such that the surface compression is balanced by internal tension. It is believed that the surface compression extends inward from each surface by about 10 percent of the web thickness. Thus, a vertical residual stress distribution such as that shown in Figure 6 can be assumed. A web surface crack that is extended into the residual

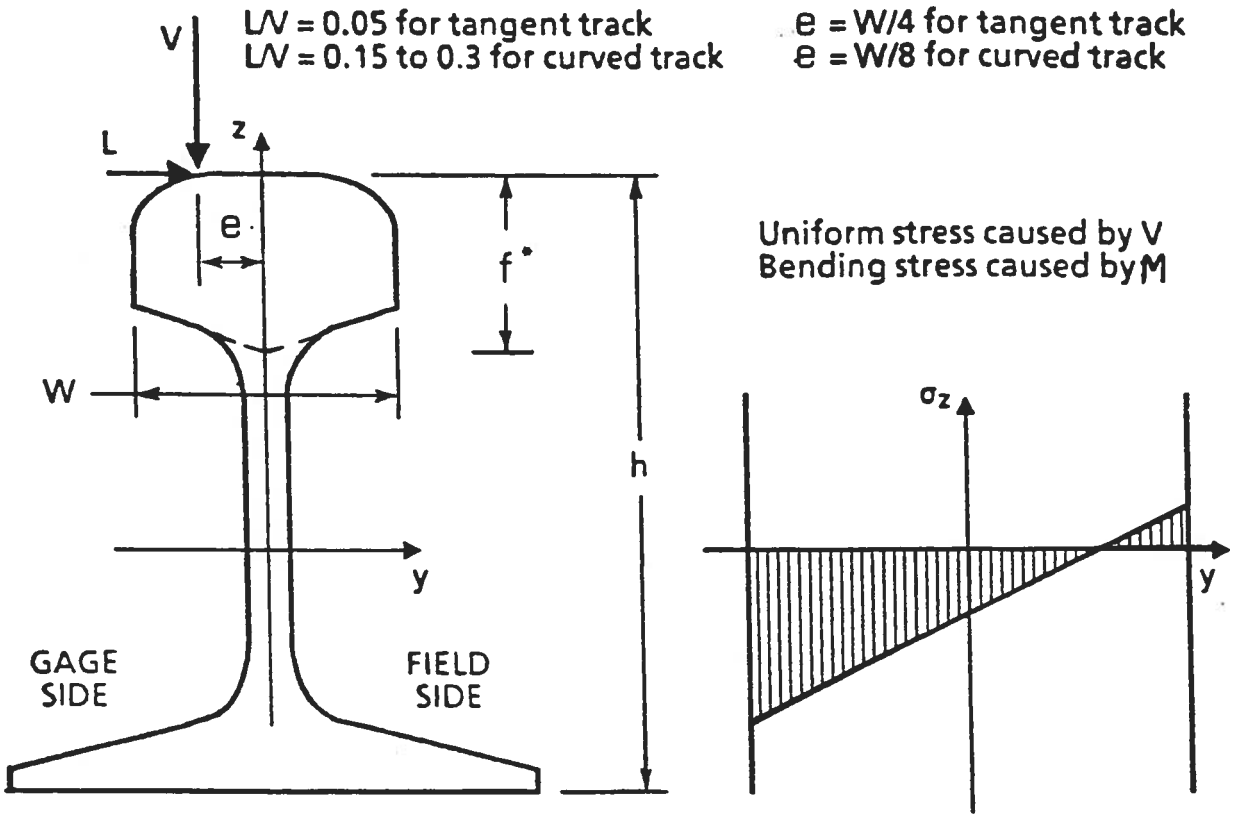

FIGURE 4. RAIL LOADED BY ECCENTRIC VERTICAL AND LATERAL WHEEL LOADING

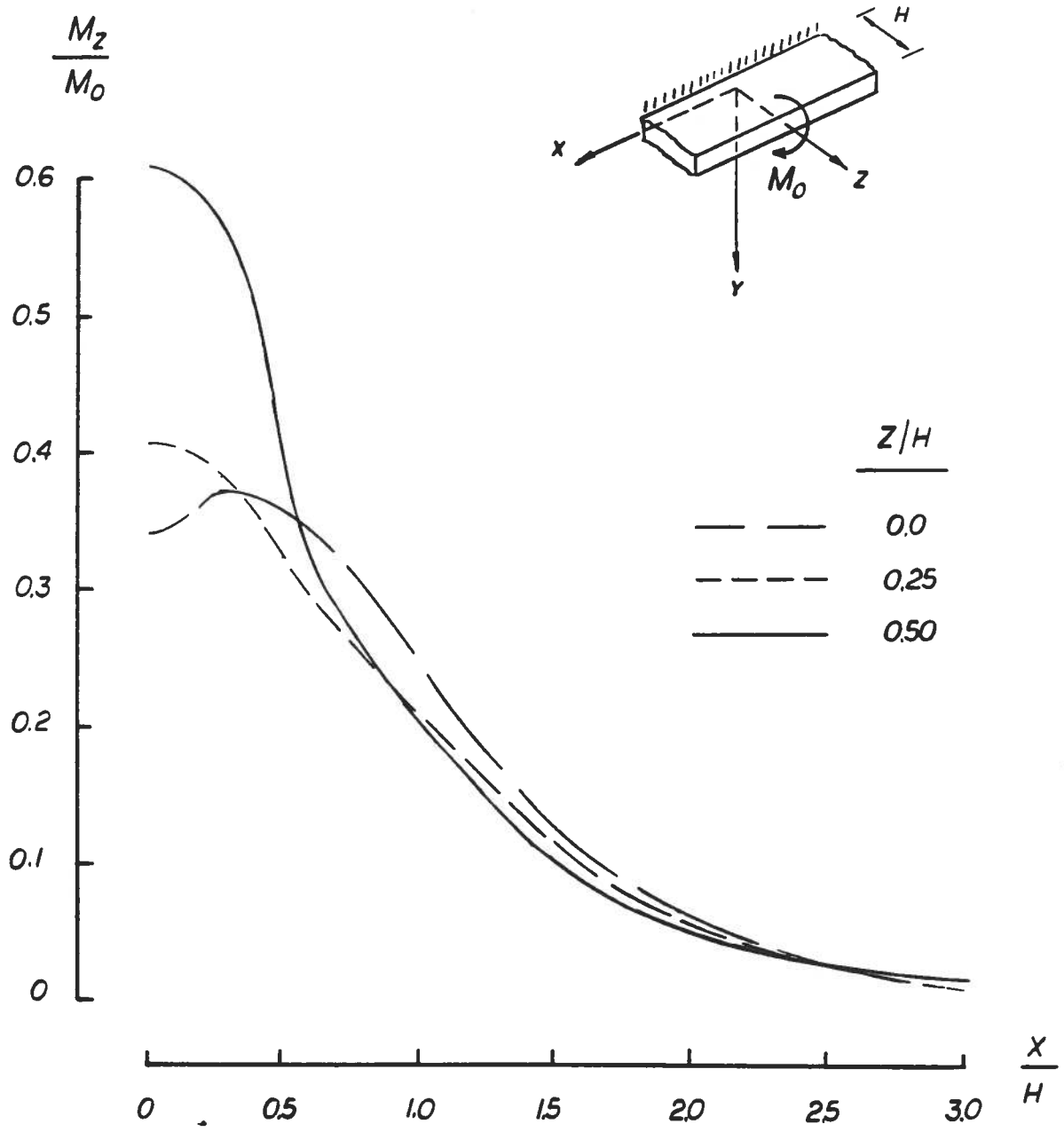

FIGURE 5 - VARIATION OF VERTICAL STRESS DUE TO ECCENTRIC VERTICAL AND LATERAL LOAD

FIGURE 5. VARIATION OF VERTICAL STRESS DUE TO ECCENTRIC VERTICAL AND LATERAL LOAD

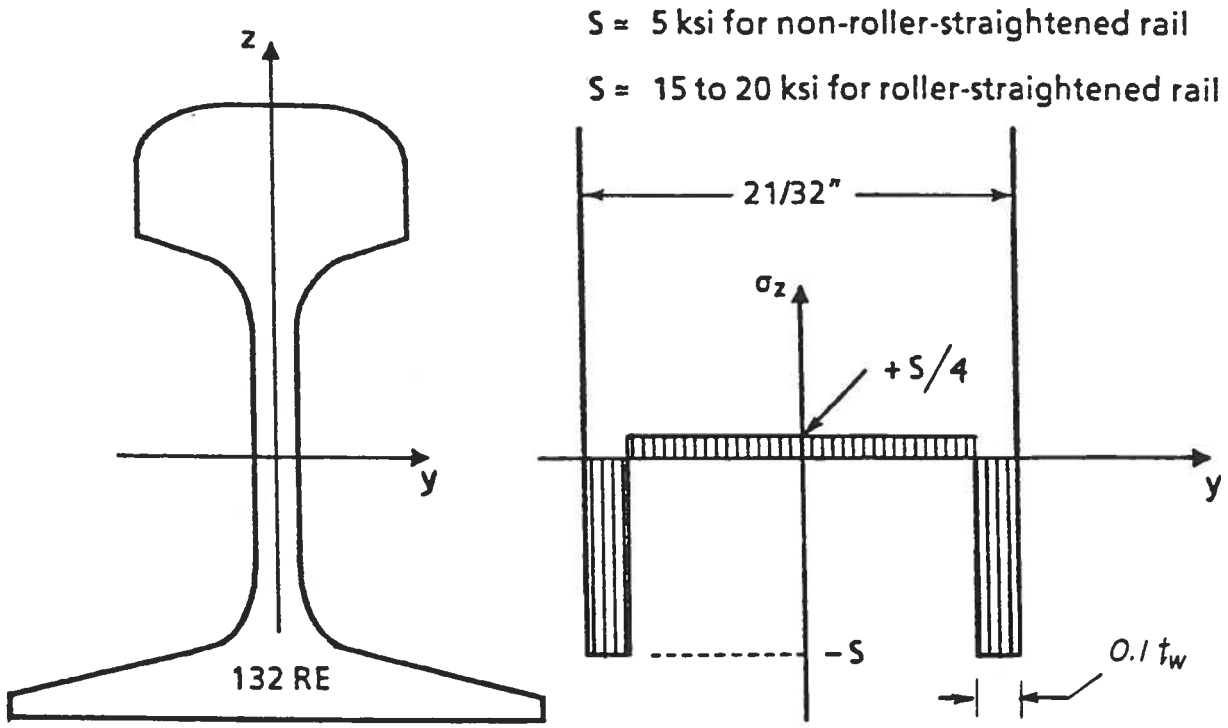

FIGURE 6. ASSUMED RESIDUAL STRESS DISTRIBUTION

tension region can grow under live traffic loads. It is important to note that the contribution of the residual stress to the calculation of the fatigue life in this model is merely to change the mean stress.

The cyclic variation of stress is assumed to be created from a single wheel load. That is, two pairs of minimum and maximum stresses result from the application of a single wheel load which can be seen in Figure 7. The magnitude of the two maximum stresses is assumed to be 0.043 times the value of the magnitude of the minimum stress beneath the applied wheel load. This factor is derived from the reversed bending due to the beam on elastic foundation formula for deflections. Also, no truncation of the stress cycle for compressive stress is assumed. This stress cycle, however, is most likely to be a more severe case than is actually experienced. The variation of the rail deflection due to a train consist type of loading is shown in Figure 8. The significance of this figure becomes evident when it is recalled that one of the components of vertical stress is proportional to the rail deflection. It can be seen that the actual vertical stress history is relatively complex compared to a single wheel load model. Therefore, in order to simplify the analysis a single wheel load is used to model the stress cycle.

2.2 CRACK GROWTH ANALYSIS

The surface crack is modeled as a semi-elliptical crack with a known aspect ratio (see Figure 9). In the present study, the aspect ratio a/2c = 0.4 is assumed. Only Mode I or the opening mode of crack growth is assumed. In order to make the analysis tractable the aspect ratio in the engineering model is assumed to be constant as the crack propagates. By invoking this assumption of constant aspect ratio, the surface crack is assumed to grow in a self-similar manner. That is, the surface crack is initially semi-elliptical in shape and remains in this same shape throughout the life of the crack. The stress intensity factor for a semi-elliptical crack is given by Reference 10 as:

$$K_I = 1.12 \frac{\sigma}{\Phi} \sqrt{\pi a} \qquad (6)$$

$$\Phi = \int_0^{\pi/2} [\, 1 - k^2 \sin^2 \theta \,]^{1/2} \, d\theta$$

$$k^2 = 1 - \frac{a^2}{c^2}$$

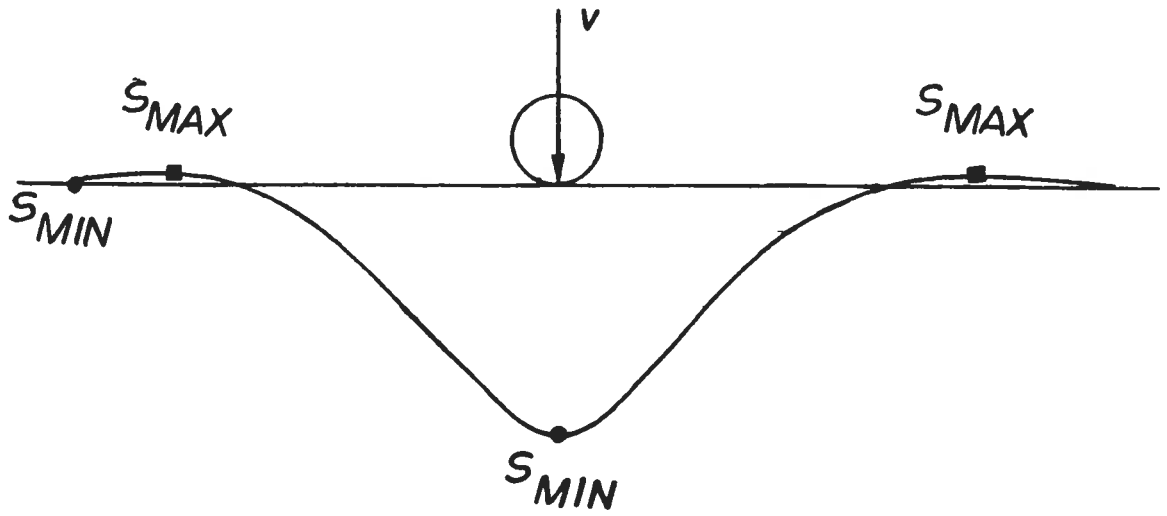

FIGURE 7. STRESS CYCLES PRODUCED BY A SINGLE WHEEL LOAD

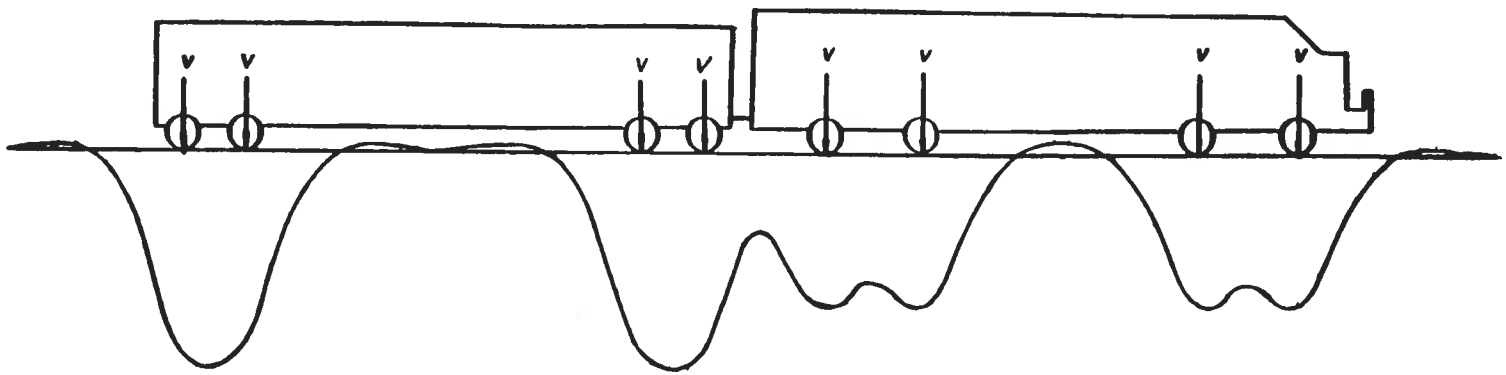

FIGURE 8. VERTICAL RAIL DEFLECTION PROFILE DUE TO MULTIPLE WHEEL LOADS

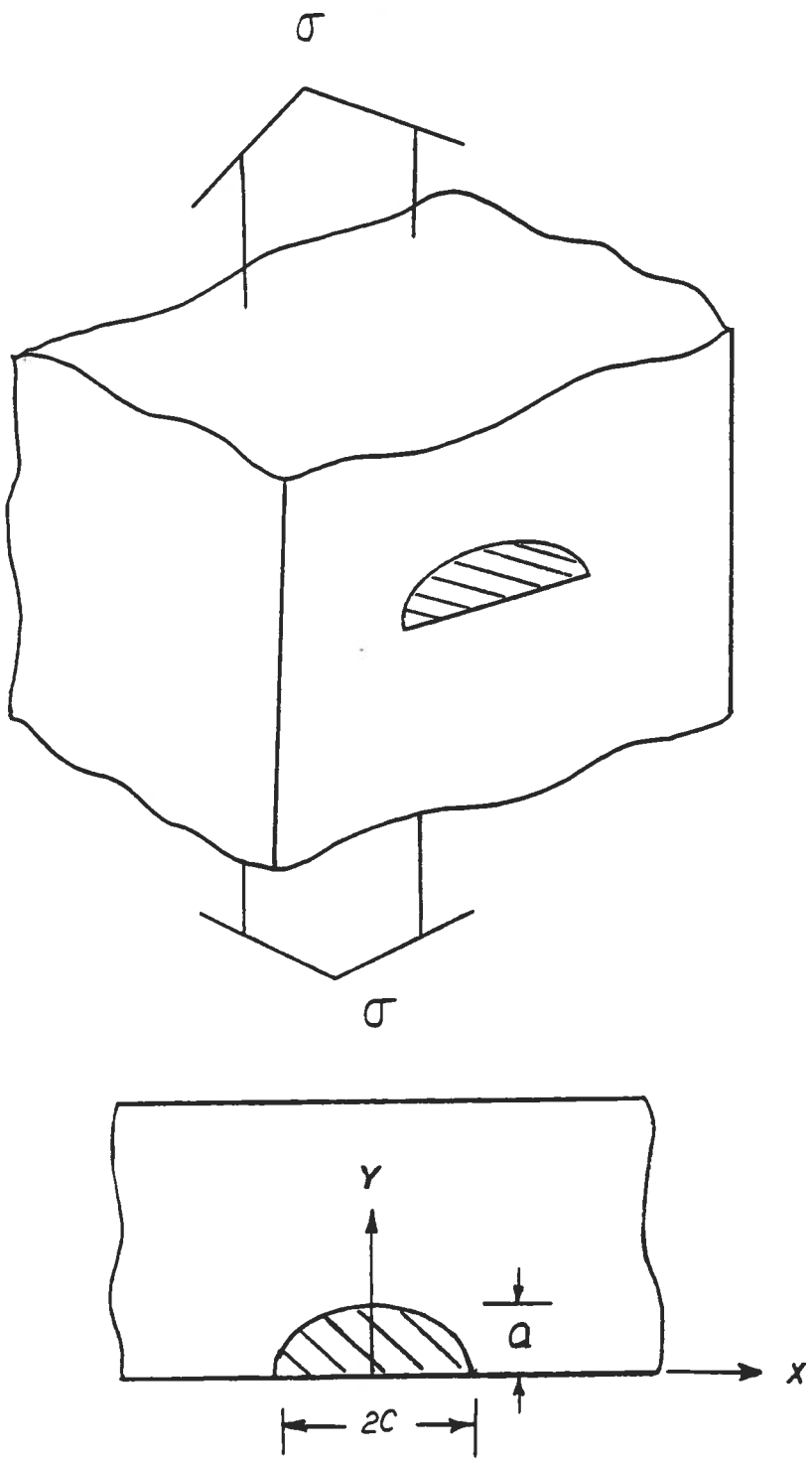

FIGURE 9. EMBEDDED SEMI-ELLIPTICAL CRACK

Corrections to the stress intensity factor due to the presence of free boundaries and to stress gradient are given for elliptically shaped cracks in Reference 11. Free surface correction factors for varying crack depths for the given aspect ratio are given in Figure 10. For fatigue loading, a crack growth law of the following form is used in the model for the semi-elliptical surface crack:

$$\frac{da}{dn} = \frac{C(\Delta K)^p}{(1-R)^q} \qquad (7)$$

where C is the crack growth rate constant, p and q are crack growth exponents, and R is the stress ratio defined as minimum stress to maximum stress in a given stress cycle. This crack growth relation was also used in the study of detail fracture in the rail head in Reference 3. Note that by including the stress ratio, R, the effect of mean stress is included. In the original form of the power law equation presented by Paris, this effect was not included [12]. Also note that three parameters in equation (7) must be determined experimentally. These parameters have been reported in Reference 13 as follows: $C = 1 \times 10^{-11}$ in. cyc.$^{-1}$ (ksi/in)$^{-p}$, p = 4, and q = 1.63.

2.3 RESULTS

A set of parameters was chosen to represent the possible track conditions on the Northeast Corridor. A surface crack on the field side of a 132RE rail was assumed to have initiated at the neutral axis of the rail. The following parameters were varied in the model (baseline values are also listed):

1) vertical foundation modulus (2500 psi),

2) track curvature in terms of L/V (0.05),

3) magnitude of residual stress (0 ksi).

A sensitivity study was performed by varying each of these parameters one at a time while the others were held at their respective baseline values. The material properties of the rail were characterized by the crack growth constants given in Reference 13, as mentioned previously. These values were not changed during the sensitivity study. Furthermore, no threshold value for the stress intensity factor was assumed. The results are presented in the form of plots showing the crack size in terms of the ratio of the semi-minor axis length to web thickness versus the number of cycles to failure. In general, for rail defects the number of cycles to failure is translated into an equivalent value for tonnage carried over the track in terms of million gross tons.

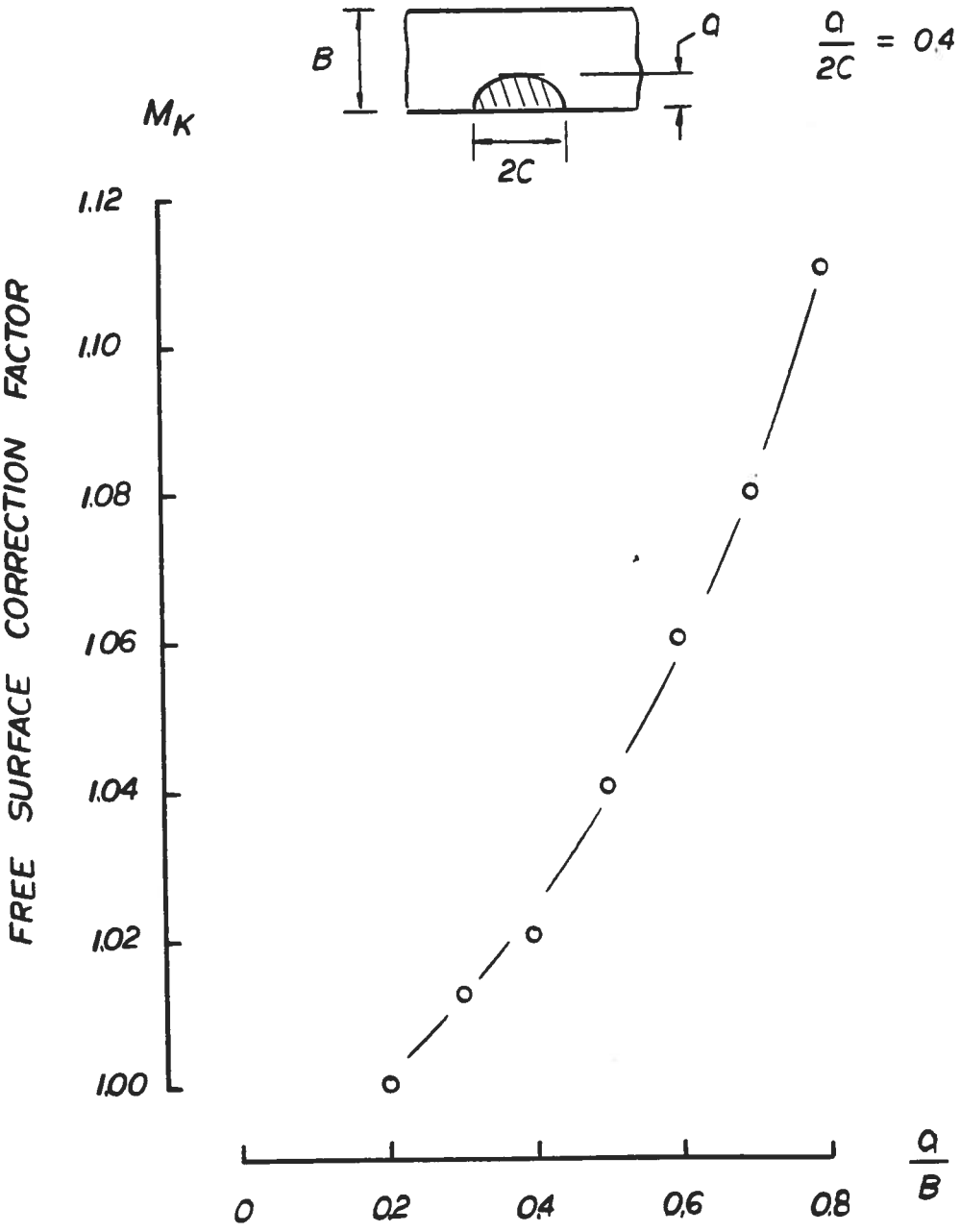

FIGURE 10. FREE SURFACE CORRECTION FACTORS

The value of the vertical foundation modulus was varied from the baseline value to 10,000 psi which represents concrete tie track. The engineering fracture mechanics model showed that the vertical foundation modulus does not affect the fatigue life of the surface crack. The model assumed that one of the contributors to the vertical stress was a uniform stress caused by the stress distribution from the vertical track and head on web moduli. The head on web effect is a highly localized effect which dominates the contribution to this component of the vertical stress as opposed to the dispersed effect of the track foundation modulus.

The effect of residual stress is shown in Figure 11 for tangent track loading and in Figure 12 for curved loading (i.e., L/V =0.30). In the tangent case, when there is no residual stress the crack growth rate is extremely slow. Tables 2 and 3 list the values of fatigue crack life for different increments of crack size and maximum residual stress. In the curved track case with no residual stress this model predicts that a web surface crack will not grow. The most conspicuous result is that the effect of increasing the magnitude of the residual stress is to increase the crack growth rate. It is also interesting to note that a reduction in the crack growth rate is apparent as the crack approaches the center of the web. This may be due to gradients in the distribution of the vertical stress through the thickness which, in turn, reduces the effective stress intensity factor.

In general, the results of the engineering fracture mechanics model show that the crack growth rates are relatively slow (as compared to the detail fracture, for example). This is consistent with the fact that the occurrence of surface cracks on the rail web are not widespread. However, it must be noted that the assumptions concerning the stress analysis were made to yield conservative predictions for fatigue life.

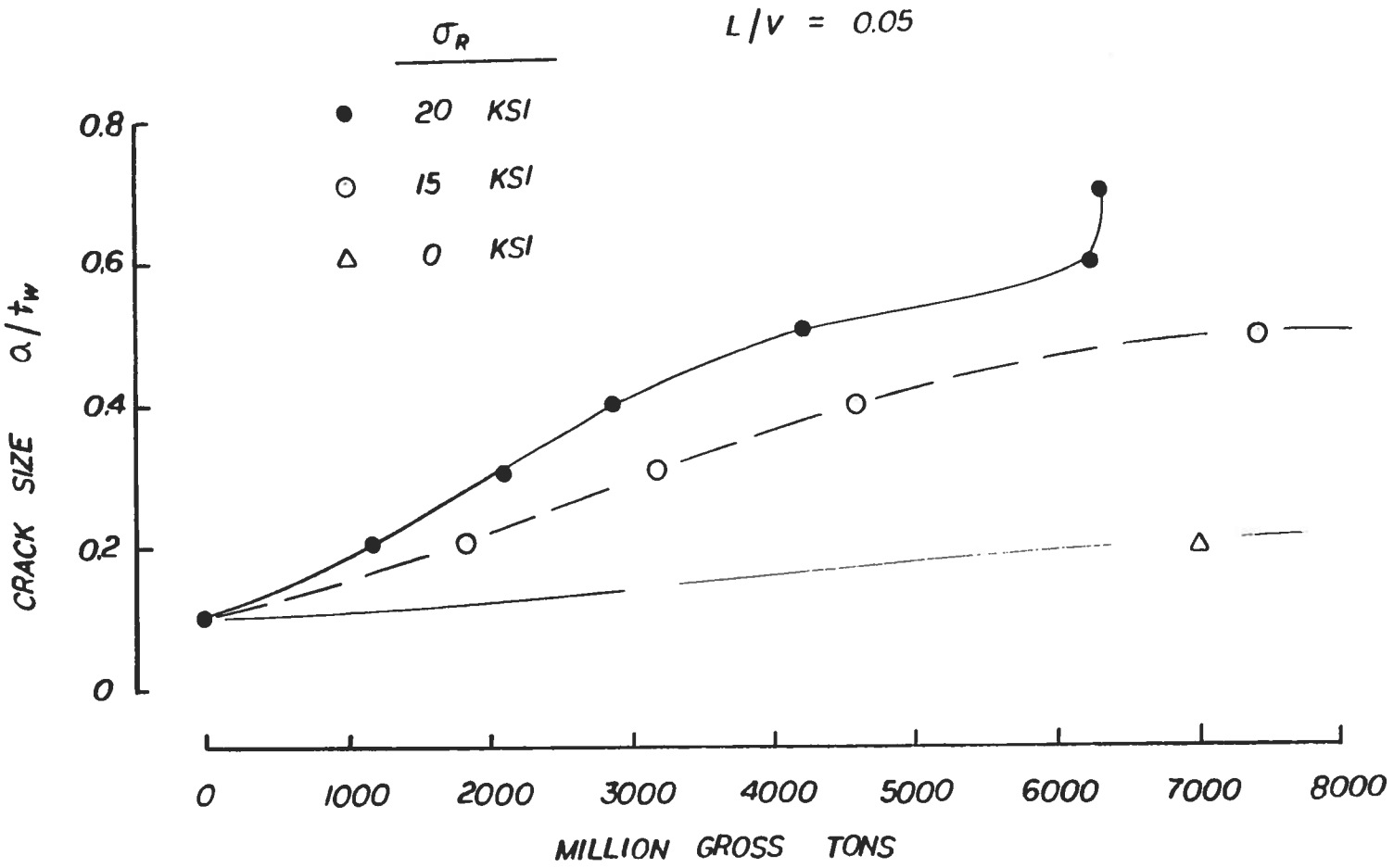

FIGURE 11. RESULTS OF ENGINEERING MODEL FOR TANGENT TRACK LOADING

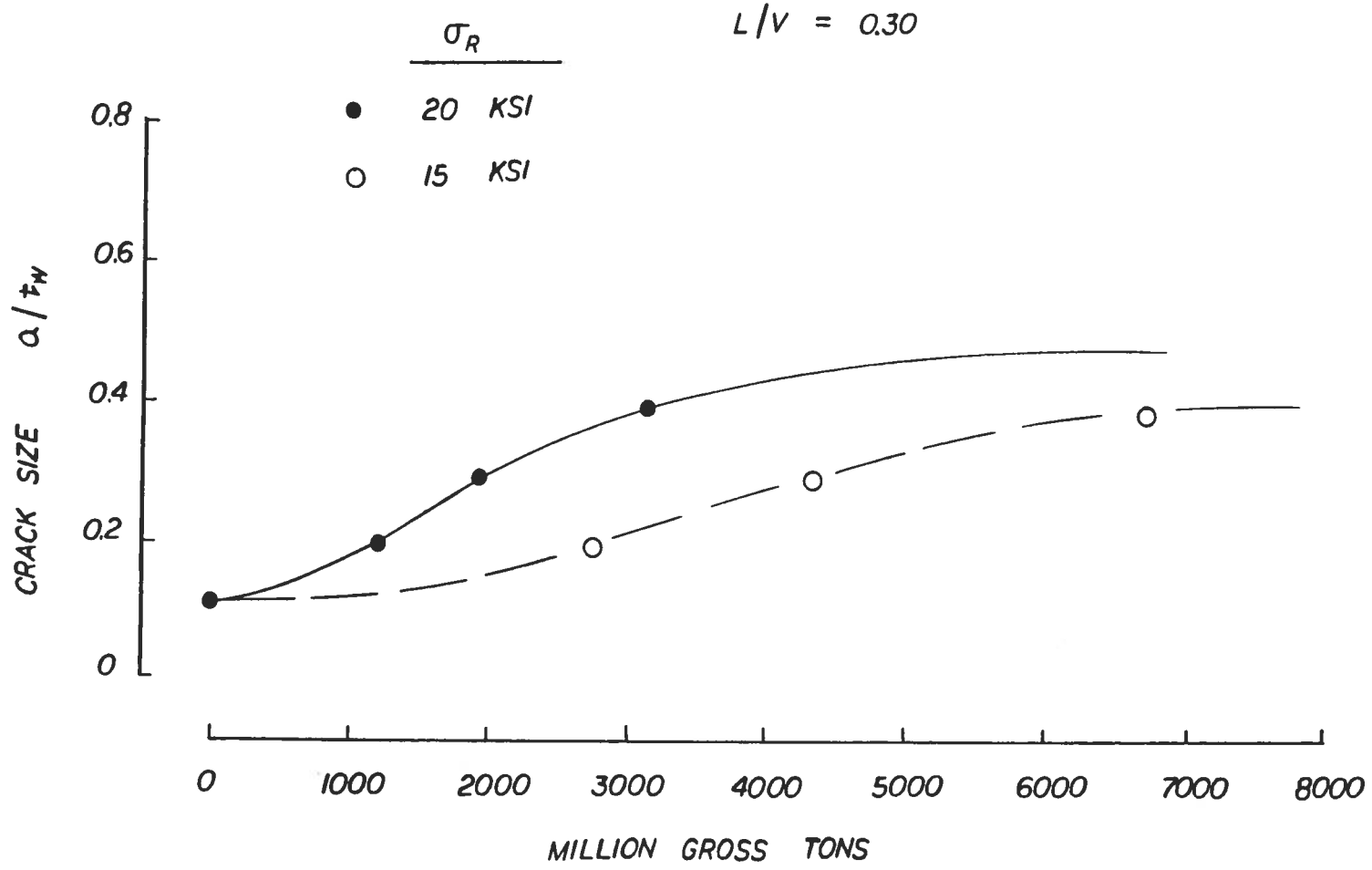

FIGURE 12. RESULTS OF ENGINEERING MODEL FOR CURVED TRACK LOADING

TABLE 2. FATIGUE CRACK GROWTH LIVES FOR TANGENT TRACK LOADING (in MGT)

Crack size	σ_r = 0 ksi	σ_r = 15 ksi	σ_r = 20 ksi
0.10 - 0.20	7039	1850	1196
0.20 - 0.30	16,518	3192	2102
0.30 - 0.40	36,013	4582	2913
0.40 - 0.50	373,370	7442	4214
0.50 - 0.60	∞	19,066	6276
0.60 - 0.70	∞	19,130	6308

TABLE 3. FATIGUE CRACK GROWTH LIVES FOR CURVED TRACK LOADING (IN MGT)

Crack size	σ_r = 0 ksi	σ_r = 15 ksi	σ_r = 20 ksi
0.10 - 0.20	∞	2751	1200
0.20 - 0.30		4336	1932
0.30 - 0.40		6735	3104
0.40 - 0.50		30,509	18,560
0.50 - 0.60		42,133	20,622
0.60 - 0.70		44,434	21,839

3. STRAIN ENERGY DENSITY MODEL

A second approach to the investigation of the growth life of a surface crack in the rail web was undertaken using the strain energy density criterion. In this model, mixed mode crack propagation is assumed, namely, Mode I and Mode III are assumed. Mode I results from the vertical wheel loading while Mode III results from the applied lateral load. Although it is not assumed in this investigation, Mode II can also be included. By excluding Mode II, the crack propagates in the same plane. If all three modes are included in a crack growth model, a true three-dimensional crack problem must be solved since the surface crack would no longer propagate in one plane. In order to simplify the analyses, the crack is assumed to grow in the same plane which is the implied assumption used in the engineering model. Another feature in the strain energy density (SED) model which differs from the engineering model is that the surface crack is allowed to grow in a non-self-similar manner. The linear fracture mechanics approach, which relied on the concept of the critical stress intensity factor, assumed that the crack grows in a self-similar fashion. In the strain energy density model, the surface crack has an original shape which is assumed to be semi-elliptical. However, as the crack propagates, the amount of crack extension is determined by the strain energy density criterion, which may not be constant along the boundary of the crack. The strain energy density criterion assumes that the material elements near the crack border can fail by energy release when a critical amount of stored energy per unit volume is reached. Figure 13a shows a schematic of the strain energy density function as a function of the radial distance from the crack border for different points on the crack front. The strain energy density function decays rapidly in the form of 1/r as the radial distance increases. The locations at which dW/dV reaches $(dW/dV)_c$ determine the shape of the crack profile for a given number of load cycles. For fatigue loading, there are two such curves for the strain energy density function at each location along the crack front, see Figure 13b. These two curves represent the maximum and minimum states which may correspond to the maximum and minimum stress states. Energy dissipated by plastic deformation occurs prior to breaking of the elements along the prospective path of macrocrack growth and, therefore, is not available at the time of macrocrack surface creation. The path dependent nature of crack growth in materials that deform beyond the yield point is described in Reference 14.

3.1 STRAIN ENERGY DENSITY CRITERION

The number of cycles required for an initially semi-elliptical shaped crack to grow into a non-self-similar

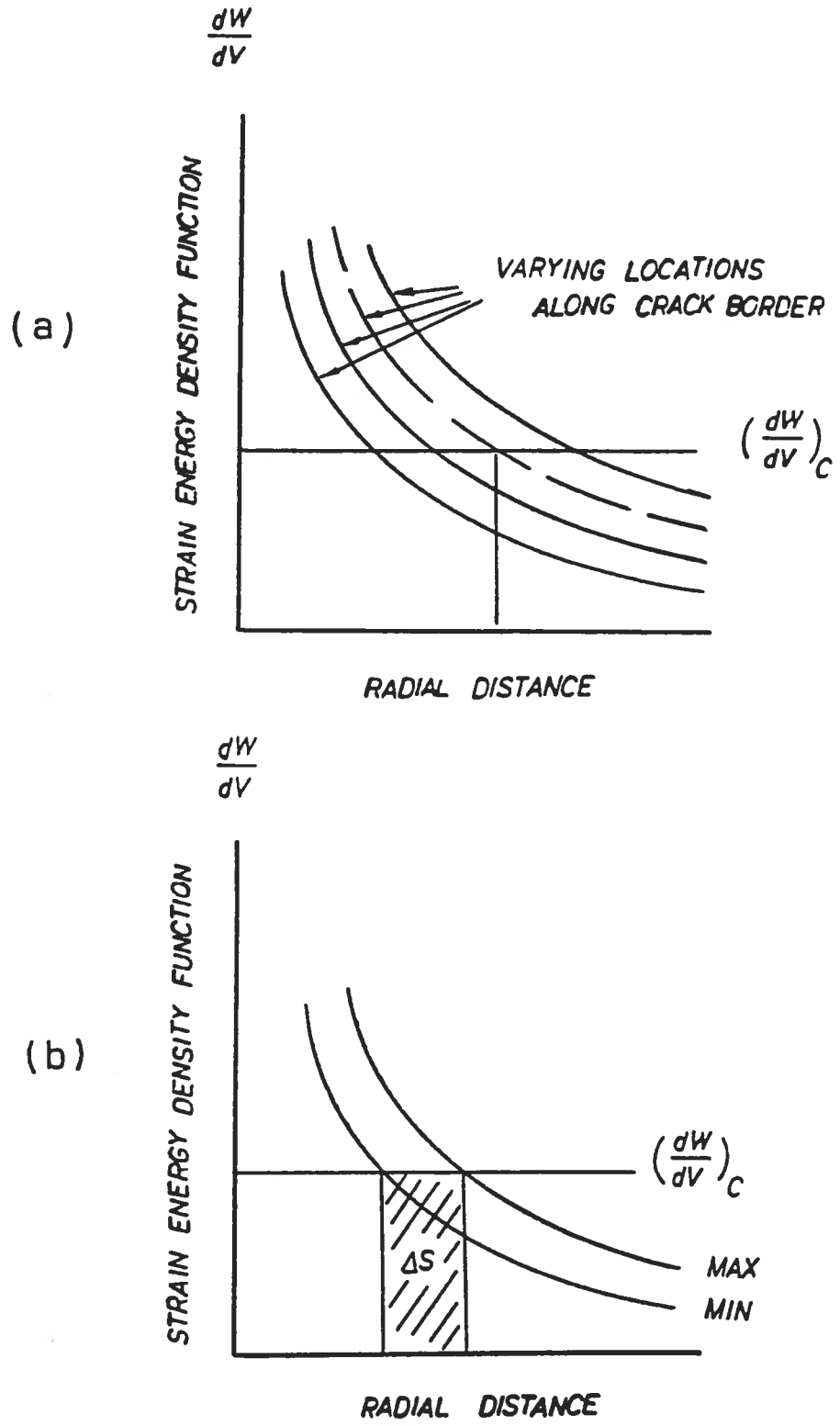

FIGURE 13. SCHEMATIC OF STRAIN ENERGY DENSITY FUNCTION WITH RADIAL DISTANCE FROM CRACK BORDER

shape and become unstable will be estimated from the strain energy density criterion. Extending the work to three dimensions, a critical value of the strain energy density function $(dW/dV)_c$ is assumed to govern the failure of material elements near the crack border in Figure 14 such that:

$$\frac{\Delta S_1}{\Delta r_1} = \frac{\Delta S_2}{\Delta r_2} = \ldots \frac{\Delta S_n}{\Delta r_n} = \text{constant} = \frac{\Delta S_c}{\Delta r_c} \qquad (8)$$

where $\Delta S_j = (S_{max} - S_{min})$ $j=1,2,\ldots n$ and S is the strain energy density factor. Referring to Figure 13b, ΔS is the rectangular area with sides $(dW/dV)_c$ and Δr which represents the segment of crack growth as the load is cycled from the minimum to the maximum state. The quotient $\Delta S/\Delta r$ is taken to be a constant along the fatigue crack front until $\Delta S_c/\Delta r_c$ is reached, at which point global instability prevails. This constant value can be evaluated from experimentally measured cyclic stress and strain curves since:

$$\frac{dW}{dV} = \frac{\Delta S}{\Delta r} \qquad (9)$$

In the present study, the critical value for the strain energy density is $(dW/dV)_c = 1358$ psi. This value for the strain energy density represents a fraction (one tenth) of the total area beneath the true stress versus true strain curve. The critical value of the strain energy density factor S_c is related to the ASTM fracture toughness K_{1c}:

$$S_c = \frac{(1 - 2\nu)}{4\mu\pi} K_{1c}^2 \qquad (10)$$

where ν is Poisson's ratio and μ is the shear modulus of elasticity.

The proposed fatigue crack growth relation has the following form [15]:

$$\frac{\Delta r}{\Delta N} = B (\Delta S)^m \qquad (12)$$

where B and m are two experimentally determined coefficients that can be determined from data for rail steel such as that from References 13 and 16. In the case of self-similar Mode I crack extension, $\Delta r/\Delta N$ becomes $\Delta a/\Delta N$ such that a single crack length dimension a is sufficient. In general, Δr in Figure 14 may vary from point to point on the crack front for each interval of load cycle ΔN of growth. The crack growth constants B and m are

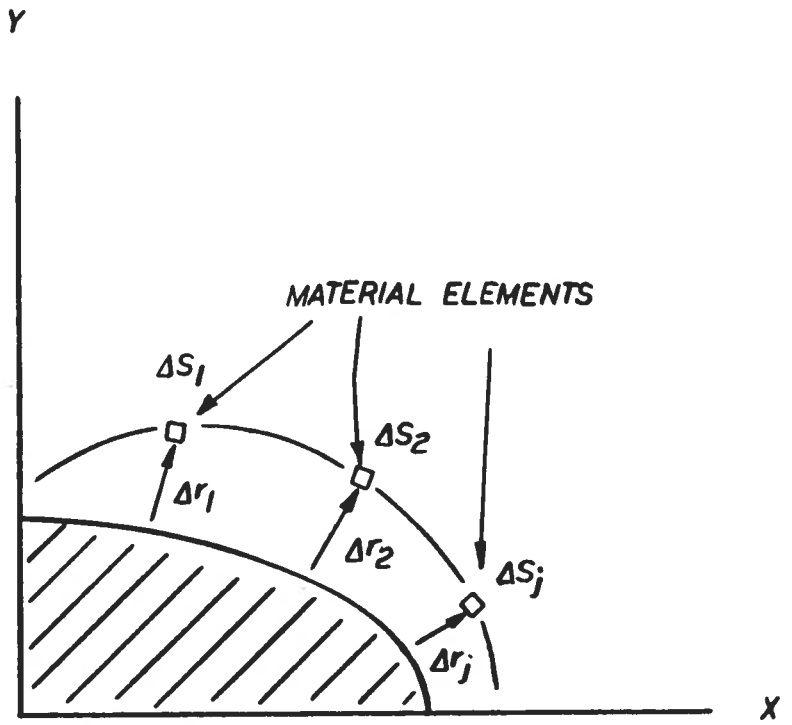

FIGURE 14. SCHEMATIC OF NON-SELF-SIMILAR CRACK GROWTH

related to the constants C and p in the engineering fracture mechanics model given by equation (7) and are $B = 1.096 \times 10^{-6}$ inches $cycle^{-1}$ $(lb/in)^{-m}$ and $m = 2$. The derivation of these values from the crack growth constants used in the engineering fracture mechanics model is given in Appendix C.

3.2 FINITE ELEMENT ANALYSIS

Three-dimensional finite element analysis is used to model the rail web with an initially semi-elliptical surface crack. The stresses in the rail web are calculated based on the usage of 20 node isoparametric elements with shape function gradients at the Gaussian quadrature points. The 1/r singular behavior of the strain energy density function near the crack can be achieved by moving the midside crack border points of the isoparametric elements to quarterpoint positions [17,18]. In order to include the influence of the entire rail structure loading conditions, the finite element analysis is divided into two parts: one for a rail section of 22 inches in length and the other for a rail section that only includes the rail web only, (see Figure 15). The length of 22 inches represents the distance between two ties in a nominal track. These two different finite element analyses will be referred to as the full rail model and the local web model, respectively. A three-dimensional displacement distribution is obtained from the full rail model and is then used to simulate the applied loading for the local web model. Symmetry about the yz-plane (recall Figure 1) is assumed. Therefore, only one-half of the web crack is modeled. Due to the paucity of available data on the three-dimensional state of residual stress in the rail web, the effect of residual stress in the strain energy density model was not included in the present study.

In the full rail model analysis, a total of 396 nodes and 72 elements were required to model a rail segment of one tie length. Figure 16 shows the finite element grid pattern for a 132RE rail cross section. A single wheel loading was assumed (which was the same assumption used in the engineering fracture mechanics model). A vertical wheel load of 33,000 lbs. was applied at midspan with an eccentricity of 0.75 inch. A lateral load was also applied at the same contact point. Two values were assumed for lateral load: 1650 lbs. corresponding to tangent track loading and 9900 lbs. corresponding to curved track loading. Bending moments were applied at the ends of the section to enforce equilibrium. These end moments were calculated based on the classical beam on elastic foundation theory using a track foundation modulus of 2500 psi [7] .

The local web model required 256 nodes and 34 elements for the three-dimensional finite element analysis. The grid pattern for the local web model is shown in Figure 17.

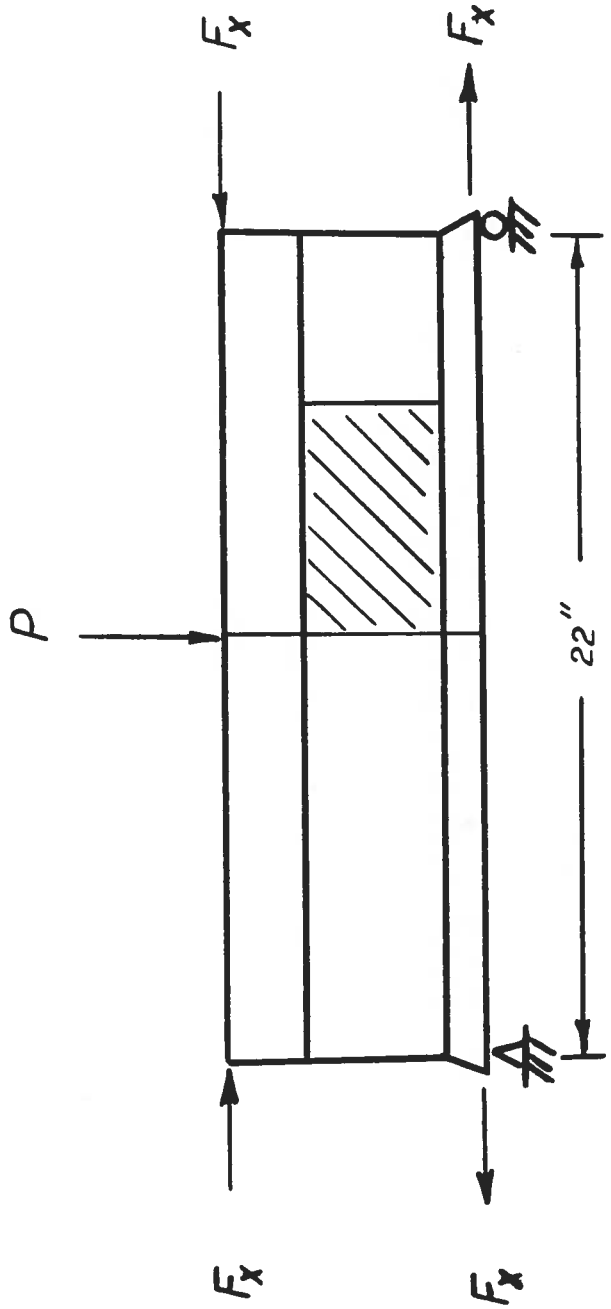

FIGURE 15. RAIL SECTION MODEL

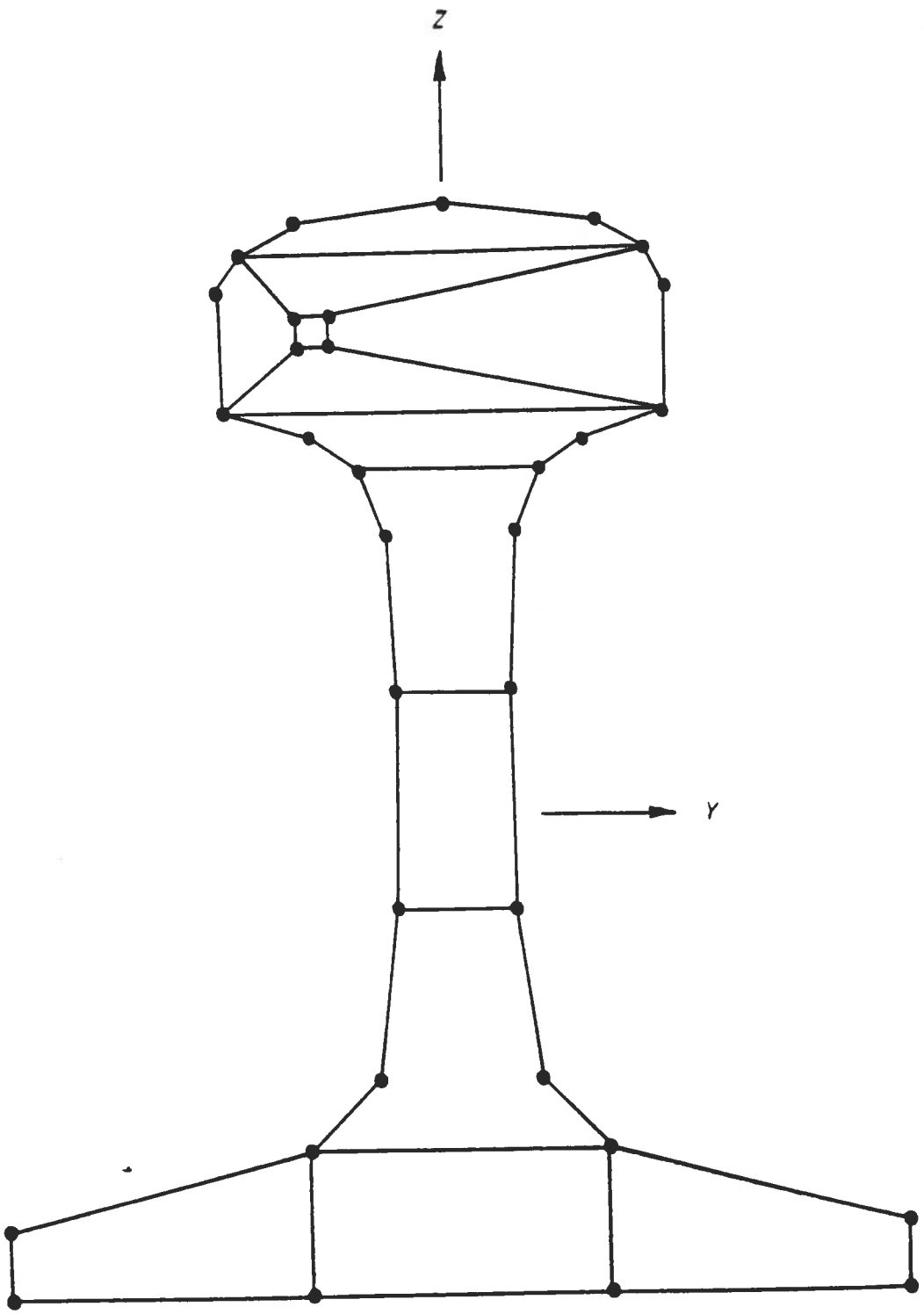

FIGURE 16. FINITE ELEMENT GRID PATTERN FOR 132RE RAIL CROSS SECTION

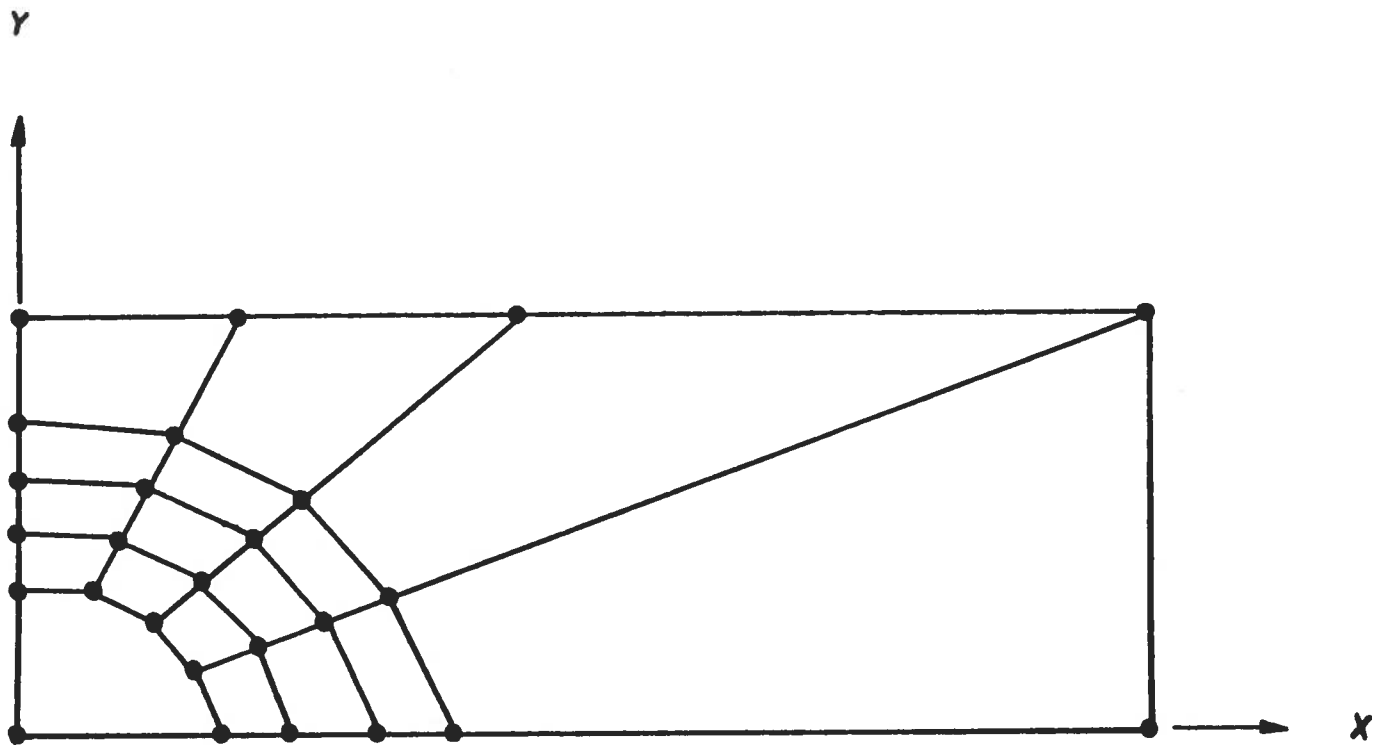

FIGURE 17. LOCAL FINITE ELEMENT GRID PATTERN FOR SURFACE CRACK IN RAIL WEB

3.3 RESULTS

Two sets of results are presented for the growth of a surface crack on the rail web located on the field side, one set for the crack subjected to tangent loading and the other for a crack subjected to curved loading (with a lateral-to-vertical load ratio of 0.30). The crack profiles for different growth increments under the tangent loading are shown in Figure 18. Note that for a single 33-kip wheel load, 3 million cycles are the equivalent to 99 MGT. It is interesting to see that the growth of the web crack is indeed non-self-similar. Furthermore, it can be seen that the crack tends to extend primarily in the longitudinal direction of the rail. Table 4 shows the values of the strain energy density range and crack growth increments for the surface crack subjected to tangent loading. Similar results can be seen for the case of curved track loading in Figure 19.

The corresponding numerical values for Figure 19 are listed in Table 5. The results from the SED model show that the curved track case has a greater crack growth rate than the tangent. This result differs from that of the engineering model which predicted no growth for the surface crack without residual stress under curved track loading.

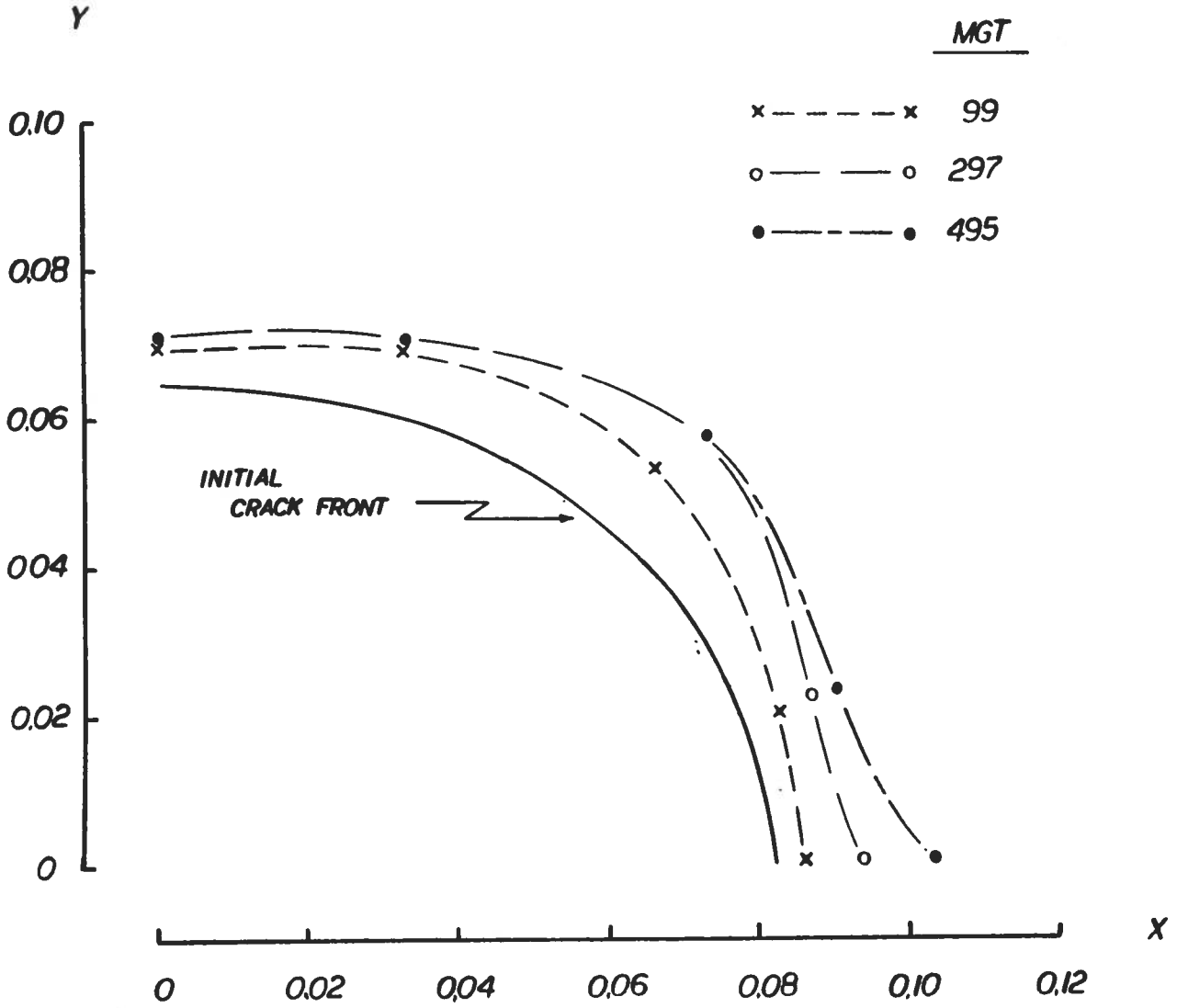

FIGURE 18. CRACK GROWTH PROFILES FOR SURFACE CRACK UNDER TANGENT TRACK LOADING

TABLE 4. RESULTS FROM SED MODEL FOR TANGENT TRACK LOADING

Crack Border Points	ΔS (lb/in x 10^{-3})	Δr (in.)
1st growth increment $\Delta N = 3 \times 10^6$ cycles		
1	37.6	0.00465
2	10.6	0.00037
3	62.7	0.01293
4	58.4	0.01121
5	33.3	0.00365
2nd growth increment $\Delta N = 6 \times 10^6$ cycles		
1	36.2	0.00862
2	36.5	0.00876
3	40.3	0.01068
4	4.4	0.00014
5	2.3	0.00003
3rd growth increment $\Delta N = 6 \times 10^6$ cycles		
1	38.9	0.00995
2	10.6	0.00074
3	7.7	0.00039
4	4.6	0.00014
5	0.0	0.0

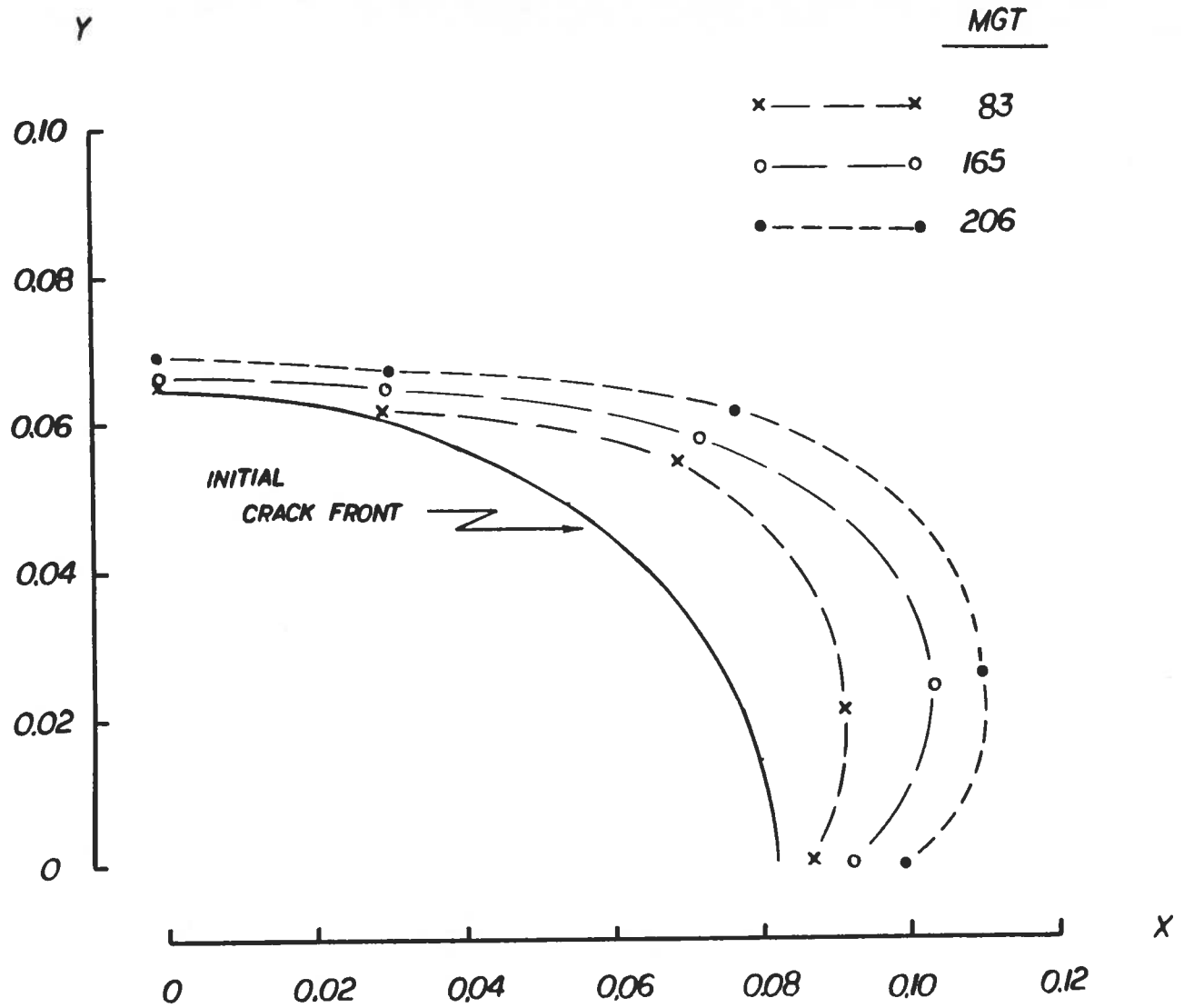

FIGURE 19. CRACK GROWTH PROFILES FOR SURFACE CRACK UNDER CURVED TRACK LOADING

TABLE 5. RESULTS FROM SED MODEL FOR CURVED TRACK LOADING

Crack Border Points	ΔS (lb/in x 10^{-3})	Δr (in.)
1st growth increment $\Delta N = 2.25 \times 10^6$ cycles		
1	42.9	0.00454
2	76.7	0.01451
3	76.5	0.01443
4	2.2	0.00001
5	2.1	0.00001
2nd growth increment $\Delta N = 2.25 \times 10^6$ cycles		
1	13.1	0.00042
2	65.1	0.01045
3	42.1	0.00437
4	32.2	0.00256
5	16.5	0.00067
3rd growth increment $\Delta N = 2.5 \times 10^6$ cycles		
1	110.8	0.01682
2	90.3	0.01117
3	79.6	0.00868
4	33.8	0.00157
5	31.7	0.00138

4. CONCLUSIONS

Two different models for determining the crack growth rate of a surface crack on the rail web have been presented. Although, these two models were developed under some different assumptions, one conclusion from the results of both models can be made: the crack growth rates are very slow; that is, to extend a crack one-tenth of an inch in any direction requires of the order of one thousand MGT. Therefore, detection of such cracks before catastrophic failure occurs should be made without much difficulty. The engineering fracture mechanics model, using only one-dimensional data, showed that the fatigue life of the surface crack is indeed sensitive to the level of the residual stress in the rail web. The predicted fatigue lives for the cases including residual stress were an order of magnitude less than those for the case without residual stress. However, the lives with residual stress are still relatively high (1196 MGT for the first ten percent of growth increment in the worst case).

The strain energy density model showed that the crack growth was non-self-similar. The crack was shown to grow primarily in the direction along the length of the rail for both tangent and curved track loading. The results from the curved case showed that the lives decreased with the increase in lateral load. In the case of tangent loading there is no growth in the thickness direction after 495 MGT. The results from the engineering model also seems to suggest that the length of the crack in the thickness direction is limited as the extension approaches the center of the web. The effect of residual stresses could not be investigated in the strain energy density model due to the lack of three-dimensional data. The study of this effect is left for future considerations.

APPENDIX A

SOLUTION OF THE CONTINUOUSLY LOADED BEAM USING FOURIER SERIES

The solution to the problem of a rectangular beam loaded continuously along the length can be found in Timoshenko and Goodier [9]. The solution is most convenient when the applied loading functions can be expressed in terms of a Fourier series. In Section 2.2, the functions for the stress distributions applied to an infinitely long beam are derived from beam on elastic foundation theory. In this appendix, these functions are transformed into series form. However, the solution in Reference [9] is given for a finite length beam. According to the beam on elastic foundation theory, a finite length beam may be treated as an infinite beam when the following condition is satisfied:

$$L > 3/\lambda_1 \tag{A.1}$$

$$\lambda_1^4 = \frac{k}{4EI_{yy}} \tag{A.2}$$

Also, E = Young's modulus, I_{yy} = area moment of inertia for vertical bending, k = rail vertical foundation modulus. The general form of the applied stress distributions is:

$$\sigma_{zz} = D\, e^{r\lambda x} (\cos \lambda x + \sin \lambda x) \tag{A.3}$$

This function can be approximated by finite Fourier cosine series:

$$\sigma_{zz} = A_o + \sum_{m=1}^{\infty} A_m \cos \left(\frac{m\pi x}{L} \right) \tag{A.4}$$

Thus, by orthogonality conditions,

$$\int_0^L A_o \, dx = D \int_0^L e^{-\lambda x} (\cos \lambda x + \sin \lambda x) \, dx \tag{A.5}$$

$$\int_0^L A_m \, dx = D \int_0^L e^{-\lambda x} (\cos \lambda x + \sin \lambda x) \cos \left(\frac{m\pi x}{L} \right) dx \tag{A.6}$$

From the integral tables, the following indefinite integrals can be found:

$$\int e^{ax} \sin bx \, dx = \frac{e^{ax}}{a^2 + b^2} (a \sin bx - b \cos bx) \qquad (A.7)$$

$$\int e^{ax} \cos bx \, dx = \frac{e^{ax}}{a^2 + b^2} (a \cos bx + b \sin bx) \qquad (A.8)$$

Therefore, the Fourier coefficient for m=0 can be solved as:

$$A_o = \frac{D}{\lambda L} (1 - e^{-\lambda L} \cos \lambda L) \qquad (A.9)$$

Also, from the integral tables it can be found that

$$\int e^{ax} \cos bx \cos cx \, dx = \frac{e^{ax} [(b-c) \sin (b-c)x + a \cos (b-c)x]}{2[a^2 + (b - c)^2]}$$

$$+ \frac{e^{ax} [(b+c) \sin (b+c)x + a \cos (b+c)x]}{2[a^2 + (b + c)^2]} \qquad (A.10)$$

$$\int e^{ax} \sin bx \cos cx \, dx = \frac{e^{ax} [a \sin (b-c)x - (b-c) \cos (b-c)x]}{2[a^2 + (b - c)^2]}$$

$$+ \frac{e^{ax} [a \sin (b+c)x - (b+c) \cos (b+c)x]}{2[a^2 + (b + c)^2]} \qquad (A.11)$$

Then for m > 0,

$$A_m = \frac{2D}{L} \left(\frac{e^{ax} [c \sin (b-c)L + (-2b+c) \cos (b-c)L] + (2b-c)}{2[a^2 + (b - c)^2]} \right.$$

$$\left. + \frac{e^{ax} [c \sin (b+c)L - (2b+c) \cos (b+c)L] + (2b+c)}{2[a^2 + (b + c)^2]} \right) \qquad (A.12)$$

APPENDIX B

CONCENTRATED MOMENT APPLIED ON A CANTILEVER PLATE OF INFINITE LENGTH

The governing differential equation from classical small deflection theory of plates is:

$$\nabla^4 w(x,y) = 0 \tag{B.1}$$

where $0 \le x \le a$, $-\infty < y < +\infty$. The solution to this equation can be expressed as:

$$w(x,y) = \int_0^\infty f(x,\alpha) \cos y\alpha \, d\alpha \tag{B.2}$$

where $f(x,\alpha) = (A + Bx) \cosh \alpha x + (C + Dx) \sinh \alpha x$ and A, B, C, and D are functions of α. The neccessary boundary conditions for the case of a concentrated moment applied at x=a are:

$$w(0,y) = \frac{\partial w}{\partial x}(0,y) = 0 \tag{B.3}$$

$$-N \left(\frac{\partial^2 w}{\partial x^2} + \nu \frac{\partial^2 w}{\partial y^2} \right)_{x=a} = \int_0^\infty \frac{2m \sin\alpha\delta}{\pi\alpha} \cos \alpha y \, d\alpha \tag{B.4}$$

$$\left(\frac{\partial^3 w}{\partial x^3} + (2 + \nu) \frac{\partial^3 w}{\partial x \partial y^2} \right)_{x=a} = 0 \tag{B.5}$$

$$N = \frac{E h^3}{12(1 - \nu^2)} \tag{B.6}$$

Then, the moment, M_x at any location in the plate is determined from

$$M_x = -N \int_0^\infty \left(\frac{\partial^2 f}{\partial x^2} - \alpha^2 \nu \frac{\partial^2 w}{\partial y^2} \right) \cos \alpha y \, d\alpha \tag{B.7}$$

The following changes in variables are introduced: $\alpha = \frac{\mu}{a}$, $\epsilon = \frac{x}{a}$, and $n = \frac{y}{a}$. Then, after a considerable amount of algebra, the moment at any normalized location in the plate is

$$M_x = - \frac{M_o}{\pi} \int_0^\infty \frac{\psi(\mu,\xi)}{\Delta(\mu)} \cos \mu\eta \, d\mu \qquad (B.8)$$

$$\psi(\mu,\xi) = - [\mu^2\xi + (\gamma+1)^2] \cosh \mu\xi \cosh \mu - \mu [\gamma + \xi(\gamma+1)] \sinh \mu\xi \cosh\mu$$

$$+ \mu [\xi\gamma + (\gamma+1)] \cosh \mu\xi \sinh \mu + [\mu^2\xi + \gamma^2] \sinh \mu\xi \sinh \mu \qquad (B.9)$$

$$\Delta(\mu) = \mu^2 + \gamma^2 + (2\gamma + 1) \cosh^2 \mu \qquad (B.10)$$

$$\gamma = \frac{1+\nu}{1 - \nu} \qquad (B.11)$$

Recall that μ is a complex number, i.e., $\mu_n = \alpha n + \iota \beta_n$. These real and imaginary roots are given in Reference 10. Then by the residue theorem,

$$\frac{M_x}{M_o} = - \mathrm{Re} \left(\iota \sum_{n=1}^{\infty} \text{residue } (\mu_n) \right) \qquad (B.12)$$

APPENDIX C

DERIVATION OF CRACK GROWTH CONSTANTS FOR THE STRAIN ENERGY DENSITY MODEL

From Section 3.1, the strain energy density function is given by:

$$\frac{dW}{dV} = \frac{\Delta S}{\Delta r} \tag{9}$$

The strain energy density factor S is related to the stress intensity factor K by:

$$S = \frac{(1 - 2\nu)}{4\mu\pi} K^2 \tag{10}$$

where ν is Poisson's ratio and μ is the shear modulus of elasticity. In terms of differences, this equation becomes:

$$\Delta S = \frac{(1 - 2\nu)}{4\mu\pi} (K_{max}^2 - K_{min}^2) \tag{C.1}$$

where $\Delta S = (S_{max} - S_{min})$. Defining $\Delta K = (K_{max} - K_{min})$ and $K_m = (K_{max} + K_{min})/2$ then equation (C.1) becomes:

$$\Delta S = \frac{(1+\nu)(1 - 2\nu)}{E\pi} K_m \Delta K \tag{C.2}$$

where E is the modulus of elasticity. Now, recall from the two parameter ΔK model:

$$\frac{da}{dn} = C (\Delta K)^p \tag{C.3}$$

from which it is implied that $K_{min} = 0$ and $K_m = 0.5\ \Delta K$ and equation (C.2) becomes:

$$\Delta S = \frac{(1+\nu)(1 - 2\nu)}{2E\pi} \Delta K^2 \tag{C.4}$$

The strain energy density model uses a crack growth relation of the following form:

$$\frac{\Delta r}{\Delta N} = B (\Delta S)^m \qquad (12)$$

In the case of self-similar Mode I crack extension, $\Delta r / \Delta N$ becomes $\Delta a / \Delta N$ such that a single crack length dimension a is sufficient. Thus, substituting equation (C.4) into equation (12) and equating with equation (C.3) results in:

$$C (\Delta K)^p = B \left(\frac{(1+\nu)(1 - 2\nu)}{2E\pi} \Delta K^2 \right)^m \qquad (C.5)$$

Upon comparison of both sides of this equation, the following relations are obtained:

$$m = p/2 \qquad (C.6)$$

$$B = C \left(\frac{2E\pi}{(1+\nu)(1 - 2\nu)} \right)^m \qquad (C.7)$$

The crack growth constants from the ΔK model as reported in Reference 13 are $C = 1 \times 10^{-11}$ in. cyc.$^{-1}$ (ksi$\sqrt{}$in)$^{-p}$ and $p = 4$. Assuming that $E = 27.4 \times 10^3$ ksi and $\nu = 0.3$, equations (C.6) and (C.7) give $B = 1.096$ in. cyc.$^{-1}$ (1000 lb/in)$^{-m}$ and $m = 2$.

REFERENCES

1. O. Orringer, J.M. Morris, and R.K. Steele, "Applied Research on Rail Fatigue and Fracture in the United States," Theoretical and Applied Fracture Mechanics 1, 23-49 (1984).

2. G.C. Sih, Handbook of Stress Intensity Factors, Institute of Fracture and Solid Mechanics, Lehigh University, Bethlehem, PA (1973).

3. O. Orringer, et al., "Crack Propagation Life of Detail Fractures in Rails," DOT-Transportation Systems Center, Cambridge, MA, DOT/FRA/ORD-88/13 (October 1988).

4. G.C. Sih and D.Y. Tzou, "Three Dimensional Transverse Fatigue Crack Growth in Rail Head," Theoretical and Applied Fracture Mechanics 1, 103-115 (1984).

5. G.C. Sih and D.Y. Tzou, "Rail-End Bolt Hole Fatigue Crack in Three Dimensions," Theoretical and Applied Fracture Mechanics 3, 97-111 (1985).

6. S.P. Timoshenko and B.F. Langer, "Stresses in Railroad Track," ASME Transactions 54, 277-293 (1932).

7. M. Hetenyi, Beams on Elastic Foundation, University of Michigan Press (1946).

8. S.P. Timoshenko and J.N. Goodier, Theory of Elasticity, McGraw-Hill, 3rd edition (1970).

9. T.J. Jamarillo, "Deflections and Moments Due to Concentrated Load on a Cantilever Plate of Infinite Length," Journal of Applied Mechanics 17, 67-72 (1950).

10. P.C. Paris and G.C. Sih, "Stress Analysis of Cracks," ASTM STP 391, 30-81 (1965).

11. A.S. Kobayashi, M. Zii, and L.R. Hall, "Approximate Stress Intensity Factor for an Embedded Elliptical Crack near to Parallel Free Surfaces," International Journal of Fracture Mechanics 1, 81-95 (1965).

12. P.C. Paris, "The Growth of Fatigue Cracks Due to Variation in Load," Ph.D. Thesis, Lehigh University (1962).

13. J.J Scutti, R.M. Pelloux, and R. Fuquen-Moleno, "Fatigue Behavior of a Rail Steel," Fatigue & Fracture of Engineering Materials & Structures 7, 121-135 (1984).

14. G.C. Sih and E. Madenci, "Fracture Initiation Under Gross Yielding: Strain Energy Density Criterion," Engineering Fracture Mechanics 18, 667-677 (1983).

15. G.C. Sih and B.M. Barthelemy, "Mixed Mode Fatigue Crack Growth Predictions," Engineering Fracture Mechanics 13, 439-451 (1980).

16. O. Orringer, et. al., "Detail Fracture Growth in Rails: Test Results," Theoretical and Applied Fracture Mechanics 5, 63-95 (1986).

17. R.D. Henshell and K.G. Shaw, "Crack Tip Finite Elements are Unnecessary," International Journal for Numerical Methods in Engineering 9, 495-507 (1975).

18. Y. Yamada, Y. Ezawa, and I. Nishiguchi, "Reconsiderations on Singularity or Crack Tip Elements," International Journal for Numerical Methods in Engineering 14, 1525-1544 (1979).